

## Protein Crystal Growth Studies in the Low-Gravity (Magnetic Levitation) Environment

Arnowitz, L., BioSpace International  
Steinberg, E., BioSpace International  
Stover, C.C., BioSpace International  
Brooks, J.S., NHMFL/FSU, Physics  
Stalcup, T.F., NHMFL/FSU, Physics

Research activities of BioSpace International that focus on the crystallization of the bovine protein Ribonuclease S (Rnase S) have been carried out on two Shuttle flights. BioSpace International now reports that space-grown crystals of Rnase S show a systematic improvement of crystalline symmetry and apparent quality over earth-grown crystals, as determined by x-ray topography<sup>1</sup>. The goal of the present work has been to see if the magnetic force environment can produce crystals of a comparable quality to space-grown crystals. (Clearly, earth-based crystallization carries a very substantial cost savings compared with a shuttle flight.)

This group has taken a novel approach to the magnetic force environment, and is also taking temperature into careful consideration. A diagram of the BioSpace apparatus is shown in Figure 1. For completeness, the example used is with a 33 T resistive magnet at the NHMFL. In the BioSpace experiment, a novel consideration was made—not only can magnetic forces provide low gravity, they can also provide an enhanced acceleration (as in a centrifuge) by placing samples *below* the magnet center, and all effective *g* values in between. As shown in Figure 1, if the magnet is run at full field, there is a distribution of effective gravity values ranging all the way from positive 6 *g*, through zero, to negative 6 *g*. In the BioSpace experiments the protein growth cells were arranged as shown along the axis of the magnet. Each cell has a growth chamber that is only a few mm<sup>3</sup> in volume, and the protein crystals in solution are significantly (<100  $\mu\text{m}$ ) smaller. Hence the radial forces may be minimized by placing the cells along the axis of the magnet (thereby minimizing the lateral forces of the growth chamber walls) and the vertical placement determines the effective *g* values.

A second consideration is the temperature gradient that becomes an issue for vertically distributed growth cells involving biological materials. High field resistive magnets are water cooled, and the water, which is chilled, comes in at the top at about 10 °C and exits at the bottom at about 40 °C. (Because of the very high water pressure and the design of the plumbing, the acoustic vibration is minimal.) Since such temperature variations can greatly affect physical processes that involve biological materials, BioSpace has designed an insert where the temperature of each of the growth cells is controlled at 20 °C individually. Preliminary protein crystal growth studies of

Rnase S were recently carried out by BioSpace in a zero *g*, 1*g*, and 2*g* configuration similar to that shown in Figure 1. Here temperature regulation at 20 °C was employed over a three-day period where a high field resistive magnet ran continuously at 16 T. The results of the first experiment were a bit surprising. They show that it is important to consider the range of effective *g* values, both zero and greater than 1 *g*. It was interesting to note that at zero *g* *no* crystals formed. The results for the other cells were as follows: at 0.5 *g* crystals of an undesirable shape formed; at 1 *g* and 1.5 *g* many 0.4 mm “normal” crystals formed, mostly against the wall of the growth chamber; at 1.5 *g* and at 2 *g* the “best” crystals; by visual inspection, of 0.6 mm in long dimension formed, but again against the growth chamber wall. At present, the x-ray topography is still in process, so the microscopic crystal quality is not yet known. Protein crystal growth, even under the most carefully controlled conditions, can be unpredictable, and further investigations are underway to determine the best conditions for crystallization in the presence of a magnetic force.

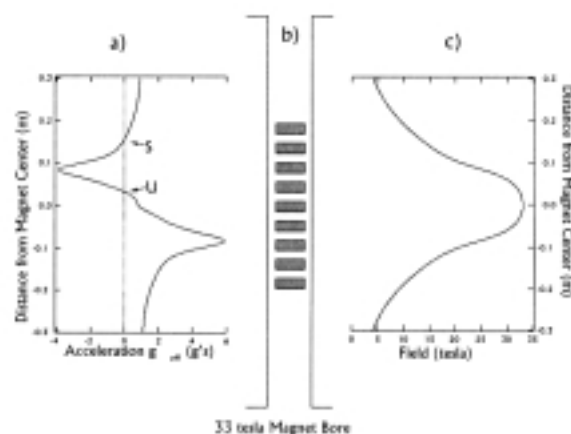


**Figure 1.** Typical field and magnetic force parameters (for water) for a 33 T, 32 mm bore resistive magnet at the NHMFL. For the case of maximum field (33 T), water-based samples can experience (as shown for different vertical displacements) an effective average body acceleration  $g_{\text{eff}}$  ranging from upwards, to zero, to downwards at six times the ambient gravitational acceleration. For *free body levitation* in this same magnet, objects such as oil, cork, and dense plastic levitate in the range 14.6, 15.6, and 16.96 T respectively at 8.7 cm above magnet center.

<sup>1</sup> Black, D., *et al.*, to be published.

## Inactivation of *Escherichia coli* and *Saccharomyces cerevisiae* Using 18 T Static and Pulsed Magnetic Field

Barbosa-Cánovas, G.V., Washington State Univ.,  
Biological Systems Engineering

Harte, F.M., Washington State Univ., Biological  
Systems Engineering

San Martin, M.F., Washington State Univ.,  
Biological Systems Engineering

The increase in demand for foods with improved and/or fresh-like quality and little heat induced degradation of nutritional and organoleptic properties gave rise to the development of nonthermal processes for the preservation of foods. Minimal thermal effect, reduced energy requirements, and potential treatment of foods inside packages had been cited as advantages for the use of magnetic field (MF) in food processing. Different mechanisms exist to explain how low intensity (mT), extremely low frequency (Hz) MF related to high voltage transmission cables and household appliances can affect physiological processes. On the other hand, reports in high intensity MF are scarce and not consistent. Our objective was to study the inactivation effect of high intensity static and pulsed MF on *Escherichia coli* and *Saccharomyces cerevisiae* under different temperature and growing media.

Pulsed MF (20  $\mu$ s, 18 T) were applied using a 7000 series Magneform machine (Maxwell Laboratories, CA). Static MF was applied using a 20 T superconducting magnet from the NHMFL at LANL. After treatment, *E. coli* was pour plated on violet red bile and nutrient agar and the resulting colony forming units were compared with bacteria receiving similar treatment but no introduced MF. The same procedure was followed for the yeast but using spread plating and potato dextrose agar.

No significant log cycle reductions were obtained when bacteria was suspended in peptoned water, McIlvaine buffer, and phosphate buffer, subjected to 50 pulsed MF at 18 T and temperature of 20, 30, 40, and 50 °C. Lack of significant log cycle reduction was also observed when bacteria was suspended in nutrient broth and phosphate buffer, and subjected to 18 T static MF for two hours at 4 and -20 °C.

Also lack of significant log cycle reduction was observed in the case of the yeast when subjected to 50 pulsed MF at 18 T and controlled temperature of 10, 20, 30 and 40 °C. Samples exposed to 18 T static MF at -20 °C two hours did not show decrease in population when compared to those at same conditions but under the influence of the geomagnetic field.

MF at strength lower or equal to 18 T has no immediate application for achieving fresh like and safe products since no significant microbial reductions were observed. More research

is needed, however, specifically at higher field strength, to draw general conclusions on this novel nonthermal technology.

## MR Studies of the Brain

Blackband, S.J., Univ. of Florida Brain Institute  
(UFBI)/UF Center for Structural Biology/NHMFL

Multiple studies at UF in both the clinical arena and the AMRIS facility seek to exploit the fundamental developments being developed in MRI both at UF and in development with the NHMFL, which are described in some of the other user reports. These developments in techniques, hardware and pulse programming/sequencing further the utility of NMR in both research and clinical studies. Several studies are progressing with a large array of clinical and basic research collaborators and with the AMRIS staff and the NHMFL supported personnel. Because these projects are oriented primarily to disease states they will not be reported in detail here; however they should be mentioned since they depend upon the progress made as described in the other reports. These disease related projects include:

### A. MR Imaging of Stroke Reduction After Estrogen Therapy in a Rat Model

J. Shi, UF, Neurological Surgery

J.D. Bui, UF, Physiology

S.H. Yang, UF, Pharmacodynamics

D. L. Buckley, UFBI, UF, Neuroscience

S.J. Blackband, UFBI, UF, Neuroscience, NHMFL

M.A. King, UFBI, Gainesville VAMC, UF, Neuroscience

A. L. Day, UFBI, UF, Neurological Surgery

J. W. Simpkins, UFBI, CAN, UF, Pharmacodynamics

Funded: NIH, Apollo BioPharmaceutics, Inc., and UFBI

This study has demonstrated that MR can detect the reduction of stroke damage in the brain after the application of neuroprotective estrogen. The effort is underway to develop clinically useful analogues of estrogen.

### B. MR Imaging and Spectroscopy of a Neonatal Rat Model of Hydrocephalus

C.M. Mohr, UF, Nuclear and Radiological Engineering

J. D. Bui, UF, Physiology

H.C. Jones, UFBI, UF, Pharmacology

S.J. Blackband, UFBI, UF, Neuroscience, NHMFL

Funded: Rudi Schulte Research Institute, NIH, and UFBI

At UF we have performed the only MR studies of a unique H-Tx animal model of hydrocephalus. Quantitative T2 and diffusion imaging techniques are being used to determine if MR is effective in evaluating the hydrocephalic brain after excess fluid is drained away, or shunted. The model provides a way to test shunting times and techniques before they are applied clinically.

### C. MRI/S of Irradiated Rats AS Model of Cortical Dysplasia and Intractable Epilepsy

L.W. Williams, UFBI, UF, Radiology  
S. Roper, UFBI, UF, Neurological Surgery  
C. M. Mohr, UF, Nuclear and Radiological Engineering  
C. Mladinich, UF, Radiology  
S J. Blackband, UFBI, UF, Neuroscience, NHMFL

Funded: Howard Hughes Foundation, NIH, and UFBI

A new model of cortical dysplasia and intractable epilepsy has been developed in rats. In these studies the utility of MR for distinguishing brain deformation and functional changes in this new model are being evaluated.

### D. fMRI of Auditory Stimulation in a Cat model at 4.7 T

P. Antoinelli, UFBI, UF, Otolaryngology  
C.M. Mohr, UF, Nuclear and Radiological Engineering  
W. King, UF, Neuroscience  
S J. Blackband, UFBI, UF, Neuroscience, NHMFL

Funded: Deafness Research Foundation and UFBI

This study is developing auditory fMRI on a cat model and complements similar auditory studies performed at UF on humans.

As just one example of the brain studies, Figure 1 shows images of a rat model of hydrocephalus where the large changes in the water content and structure of the brain are evident after shunting. The information we obtain described in other user reports, particularly on biexponential diffusion, is being used to further develop and interpret MR studies of hydrocephalus.

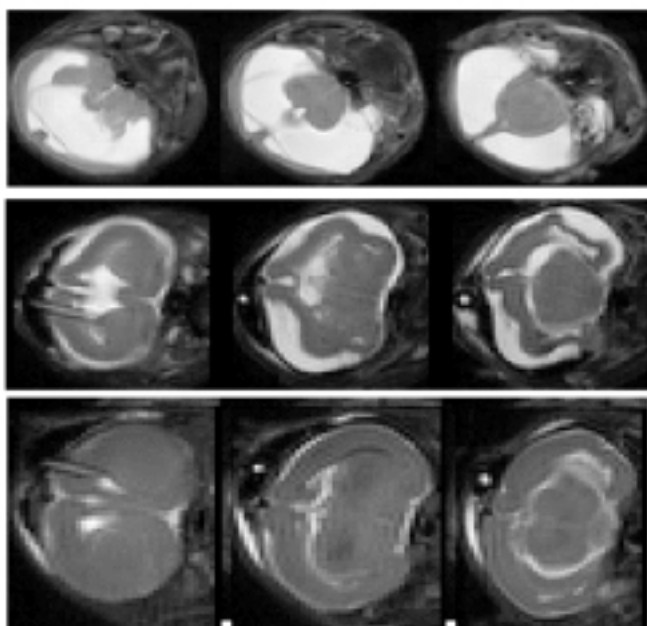


**Figure 1.** Three slices (left to right) through a hydrocephalic rat brain at (top to bottom) pre-shunt, 1 day post-shunt and 6 days post-shunt.

## NMR Microscopy and Spectroscopy of Single Cells **IHRP**

Blackband, S.J., Univ. of Florida Brain Institute  
(UFBI)/UF Center for Structural Biology/UF,  
Neuroscience/NHMFL

Grant, S., Univ. of Chicago, Bioengineering

Webb, A., Univ. of Illinois, Electrical and Computer  
Engineering

Gibbs, S., NHMFL/FAMU-FSU College of Engineering

Plant, D., UFBI, UF

Mareci, T., UFBI/UF, Biochemistry/NHMFL

Studies on single neurons isolated from the marine gastropod *Aplysia californica* have continued through the second year of an NIH grant. Using microcoils developed by Drs. Webb and Grant the first spatially localized  $^1\text{H}$  spectra of the osmolyte and metabolite content of a single cell was obtained (see figure) with a localized volume of 10 nanoliters.<sup>1</sup> The spectra show osmolytes betaine and choline at relatively high concentration that occurs in aquatic organisms. Notable is the absence of NAA, which is only found in mammalian cells. The spectral intensity is seen to deteriorate over hours in these unperfused cells, an observation consistent with cell swelling. A perfusion system is required to maintain the cells. A publication is under review.

We have also obtained the first  $^{23}\text{Na}$  images of a single cell. The images take a few hours to obtain precluding dynamic studies at present, but are similar in appearance to  $^1\text{H}$  images (albeit it at lower spatial resolution) in that the nucleus is hyperintense indicating a longer  $T_2$  for  $^{23}\text{Na}$  in the nucleus compared to the cytoplasm.<sup>2</sup> More cells must be examined before publication.

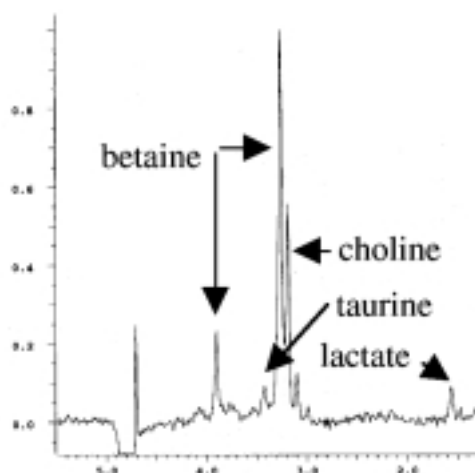


**Figure 1.**  $^1\text{H}$  spectrum from a single *Aplysia* neuron.

Our latest studies have examined the diffusion coefficient (D) of water in the cells and we have observed for the first time a non-monoexponential D within the cytoplasm, indicating multiple water compartments within the cell.<sup>3</sup> This observation has great implications for the interpretation of the observed multiexponential water D in whole tissues.

Acknowledgements: This research was supported by the NHMFL In-House Research Program, NIH, and UFBI.

<sup>1</sup> Grant, S.C., *et al.*, ISMRM 7<sup>th</sup> Annual Meeting, Philadelphia, May (1999).

<sup>2</sup> Grant, S.C., *et al.*, ISMRM 7<sup>th</sup> Annual Meeting, Philadelphia, May (1999).

<sup>3</sup> Grant, S.C., *et al.*, accepted to ISMRM (2000).

## NMR Microscopy of Isolated Perfused Brain and Heart Slices

Blackband, S.J., Univ. of Florida Brain Institute  
(UFBI)/UF Center for Structural Biology, UF,  
Neuroscience/NHMFL

Bui, J.D., UF, Physiology

Buckley, D.L., UFBI, UF, Neuroscience

Forder, J.R.F., Univ. of Alabama, Medicine

Phillips, M.I., UFBI/UF, Physiology

Studies continue examining the NMR characteristics of isolated perfused brain slices as a model of tissues. We have observed non-monoexponential diffusion in the slices and have modeled the data as being from two compartments (biexponential) corresponding to the intra and extracellular compartments.<sup>1</sup> These compartments are seen to change in accordance with this model when cell swelling is induced by the action of ouabain<sup>1</sup> or the neurotransmitter NMDA.<sup>2</sup> The effect of NMDA is negated when the tissue is first exposed to the NMDA blocker MK-801, demonstrating that the effects observed result from direct neural stimulation.

Separate studies examine slices after perfusion with Gd-DTPA contrast agent, which provides an alternative measure of the relative intra and extracellular compartment sizes. An example is shown in the Figure 1. The relative compartmental sizes are in broad agreement with the biexponential water diffusion measures adding confidence to the model.<sup>3</sup> We are now considering the implications our recent studies on single cells have on this model, since we have observed multiexponential water diffusion within single cells.

We have also performed similar studies on isolated perfused heart tissue slices, showing for the first time biexponential water diffusion within heart tissue<sup>4</sup> (manuscript submitted). Following this observation the first biexponential diffusion tensor maps of whole isolated rat hearts were obtained. The

utility of these data for differentiating normal from diseased tissue will be examined.

Acknowledgements: This work was supported by NIH and UFBI.

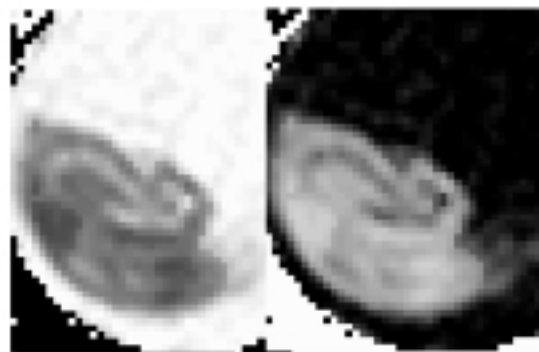


**Figure 1.** Calculated maps of the extra (left) and intracellular (right) compartments in a brain slice.

<sup>1</sup> Buckley, D.L., *et al.*, Magn. Reson. Med., **41**,137-142 (1999).

<sup>2</sup> Bui, J.D., *et al.*, (NMDA) Neuroscience, **93**, 2, 487-490 (1999).

<sup>3</sup> Buckley, D.L., *et al.*, Magn Reson Med, In Press (1999).

<sup>4</sup> Forder, *et al.*, submitted ISMRM (2000).

## A Combined High Field and Pulsed EPR Study of the Primary Donor in *Rhodobacter sphaeroides*

Bratt, P.J., UF, Chemistry

Wang, Q., UF, Chemistry

Scheer, H., Botanisches Institut, Universität München,  
Germany

Maniero, A.-L., NHMFL

Brunel, L.-C., NHMFL

Bubbenzer-Hange, C., Botanisches Institut, Universität  
München, Germany

Angerhofer, A., UF, Chemistry

ESEEM (electron spin echo envelope modulation) and pulsed ENDOR (electron nuclear double resonance) in the X-band combined with submillimeter high field CW-EPR studies were performed on the primary electron donor radical cation in *Rhodobacter sphaeroides*, P<sub>865</sub><sup>+</sup>. It was found that the electron distribution on the bacteriochlorophyll dimer (special pair) of the primary electron donor can be controlled by using different detergents for the preparation. The ratio of the spin density between the L- and M-side of the special pair was either close to 5:1 or 2:1, which indicates different conformations. In particular, it could be demonstrated that P<sub>865</sub><sup>+</sup> may be found exclusively in the 5:1 conformation at very low temperatures. The three different types of detergent used were LDAO (lauryldimethyl amine-N-oxide), BOG ( $\beta$ -octylglucoside), and SB12 (sulfobetaine-12). The pulsed ENDOR spectra showed that the



spin density distribution ratio at low temperatures is independent of detergent preparation and is always found in the highly asymmetric 5:1 conformation. Even more surprisingly, we find that the anisotropic  $g$ -matrix as measured from the  $g$  values in high magnetic fields is invariant over the temperature range studied, 5-150 K. This suggests that the delocalization of the electronic wave function of  $P_{865}^{+}$  has been reduced to the point where  $g$  is not any more sensitive to structural changes as they occur in the special pair with increasing temperature.

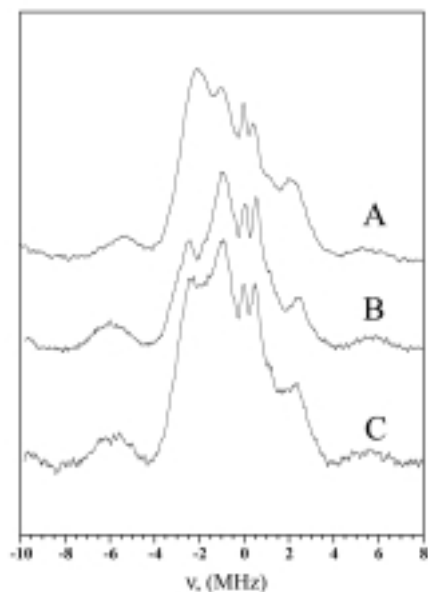


**Figure 1.** A comparison of the Mims ENDOR spectra of light oxidized  $P_{865}^{+}$  using the three different detergent preparations. Spectroscopic conditions:  $\tau = 112$  ns; microwave frequency was 9.72 GHz; number of scans: 30; shots per point: 25; static field: 3466 gauss; sweep width: 5-23 MHz. The Larmor frequency of the free protons has been set as the center of the spectrum at 14.7 MHz. (A) BOG; (B) SB12; (C) LDAO.

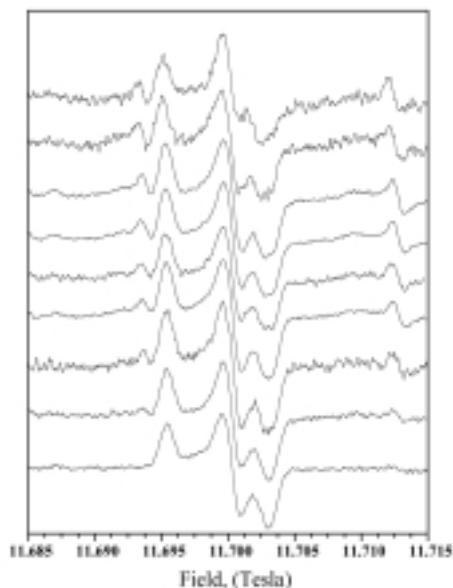


**Figure 2.** The temperature dependence of the  $P_{865}^{+}$  high field EPR signal. The spectral parameters were: Microwave frequency: 328.056 GHz; modulation frequency 8.6 kHz; modulation amplitude: 0.5 - 1.5 mT.

## High Definition Structure of a Proton Wire

Busath, D., Brigham Young Univ., Zoology

Phillips, L.R., BYU, Zoology

Cole, C., BYU, Zoology

Hendershot, R.J., BYU, Zoology

Cotten, M., NHMFL/FSU, Chemistry and Molecular Biophysics

Cross, T.A., NHMFL/FSU, Chemistry and Molecular Biophysics

Proton transport on water/protein wires is fundamentally important to many processes in biology. Here, the structure and kinetics of gramicidin A channel analogs are characterized yielding important new insights.<sup>1</sup> Fluorine substituted tryptophans have been incorporated into gramicidin in place of native tryptophans to characterize the influence of dipoles on channel conductance. Detailed structural analysis of the indoles has been accomplished using solid state NMR derived orientational constraints from the perdeuterated-fluoro-Trp gramicidin analogs incorporated into uniformly aligned lipid bilayers. The dipoles within the indole ring of the tryptophan side chains have been calculated using *ab initio* calculations.<sup>2</sup> The solid state NMR data orients the indole rings with respect to the magnetic field direction and the bilayer normal and in this way the fluoro-tryptophan dipole magnitude and orientation with respect to the conductance pathway is determined.

In symmetrical 0.1 N HCl solutions, fluorination of Trp-11, Trp-13, or Trp-15 sidechains (increasing the side chain dipoles) is found to inhibit proton conductance. Replacement of one or more Tryptophans with Phenylalanine (lacking a side chain dipole) enhances proton transport. This is the opposite effect observed for  $K^{+}$  transport in similar phosphatidylcholine bilayers. The current-voltage relations are superlinear, indicating that some membrane field-dependent process is rate limiting. The interfacial dipole effects are usually assumed to affect the rate of cation translocation across the channel. For proton conductance, however, water reorientation after proton translocation is anticipated to be rate limiting. We propose that the findings reported here are most readily interpreted as the result of dipole-dipole interactions between channel waters and polar side chains or lipid headgroups. In particular, if reorientation of the water column begins with the water nearest the channel exit, this hypothesis explains the negative impact of fluorination and the positive impact of headgroup dipole on proton conductance. Water reorientation is thought to be rate limiting for Grotthus conductance in water wires. Modulation of the intrachannel water reorientation rate, defined here as the dipole/water-dipole interaction model, provides a successful qualitative explanation of the dipole effects.

<sup>1</sup> Phillips, L.R., *et al.*, Biophys. J., **77**, 2492 (1999).

<sup>2</sup> Cotten, M., *et al.*, Biochemistry, **38**, 9185 (1999).

## Magnetically-Coupled Optical-Based Noninvasive Glucose Monitoring System

Chen, C.-J., FAMU-FSU College of Engineering

Haik, Y., FAMU-FSU CoE

Pai, V.M., FAMU-FSU CoE

In diabetes, the human body is not able to automatically control blood glucose. To make up for this, a person with diabetes has to check blood sugar regularly, and adjust treatment accordingly. According to the National Institutes of Health, about 14 million people in the United States have some form of diabetes, although only half are diagnosed.

Self-monitoring of blood glucose is essential to maintain the blood sugar levels within normal ranges. The currently available commercial, FDA-approved, approach to monitoring blood glucose has been primarily invasive. In this, a drop of blood, usually from the finger tip, is taken by means of a lancet, and placed on specially coated strips. The blood glucose is subsequently obtained by reading the strips, either visually or, more frequently and accurately, by means of blood glucose meters. This approach can be extremely painful, however, and is also very inconvenient for diabetic patients, especially children.

Utilization of optical means to enable noninvasiveness in glucose monitoring has been pursued by several research teams over the last few years. Such techniques have included using near infrared and far infrared wavelength light radiation to shine on a body organ, and using the scattered or reflected light to determine, quantitatively, the glucose content in the blood stream. To date, however, these techniques have suffered from the extremely low signal-to-noise ratio (SNR) for the glucose molecules in the blood stream.

Experiments were conducted at the NHMFL into studying the optical absorption spectrum for whole blood in the fasting and the post-prandial situations. The absorption spectrum in the visible region of the electromagnetic spectrum was measured at 0, 4, and 8 T. Figures 1 and 2 show the absorption of whole blood under fasting and post-prandial situation respectively.

A significant shift is observed in the absorption intensity of the blood sample with the addition of the magnetic field. The changes in the absorption intensities for the fasting and non-fasting cases differ dramatically. It is obvious, however, that the absorption intensity is enhanced for low glucose level in whole blood as compared to higher glucose levels. The enhancement in the signal is dramatic even at 4 T. It is anticipated that lower values of glucose will yield a higher magnetically enhanced signal which will allow lower magnetic fields (of the range of 1 to 2 T) to be used for the readings.

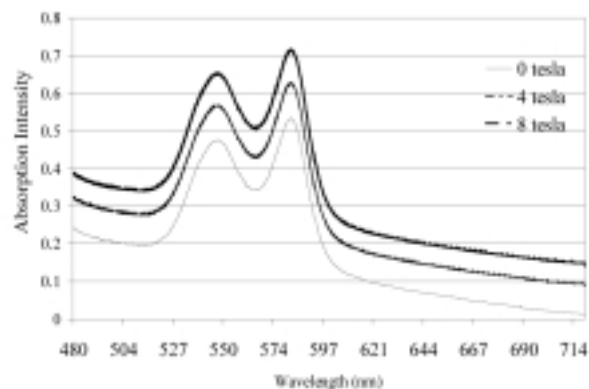


Figure 1. Fasting whole blood absorption spectrum in magnetic fields.

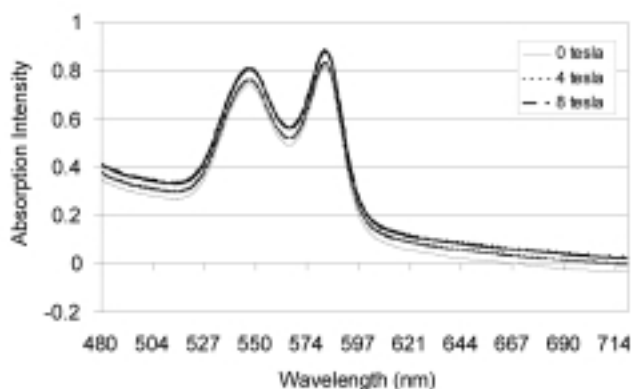


Figure 2. Post-prandial whole blood absorption spectrum (after 1 hr. of sugar intake) in magnetic fields.

## MR Microimaging Studies of Alginate Beads for Cell Encapsulation

Constantinidis, I., Emory Univ., Radiology

Grant, S.C., Univ. of Chicago, Bioengineering

Stabler, R.C.C., Emory Univ., Radiology

Long, Jr., Emory Univ., Radiology

Blackband, S.J., Univ. of Florida Brain Institute/UF Center for Structural Biology, Neuroscience/NHMFL

Alginate has been used as the vehicle to encapsulate a variety of biological materials including enzymes, and cells of both microbial and mammalian origin. In tissue engineering, and particularly in the development of a bioartificial pancreas, alginate has been employed extensively to encapsulate islets as well as transformed  $\beta$ -cells. In these new studies, we examined the effects of various alginate compositions on the growth characteristics of encapsulated  $\beta$ TC3 cells, and demonstrate the potential of MR microscopy for monitoring the distribution of cell growth non-invasively. To perform the MR studies requires high spatial resolution and sensitivity. To achieve this studies were performed using microcoils developed for the 600 MHz instrument at the NHMFL previously used in single cell studies.

Our data so far<sup>1</sup> have shown that (1) Changes in alginate composition can have a dramatic effect on the metabolic activity of the encapsulated cells, (2) T2 measurement of the alginate matrix does not reflect the rigidity of the matrix, (3) <sup>1</sup>H microimaging can be used to locate the position of cell clusters and thus non-invasively assess the distribution of cell growth in different beads. Figure 1 shows diffusion weighted images (resolution of 40x40x200  $\mu$ m) where the bright spots indicate small islands of cells. This bead was unperfused for this study. We are now in the process of developing a perfusion system so that these studies can be extended to metabolic investigations using spectroscopy.

**Acknowledgements:** This work was supported by NIH, NHMFL, and UFBI.

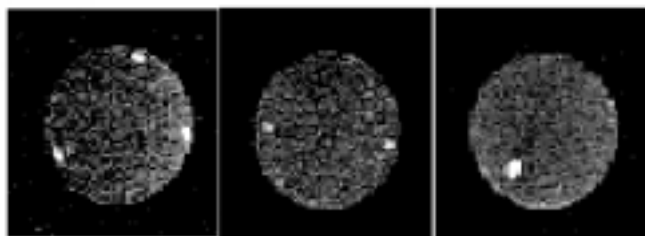


**Figure 1.** D weighted microimages (three slices) of an alginate bead encapsulating  $\beta$ TC3 cells.

<sup>1</sup> Constantinidis, *et al.*, submitted to ISMRM Proceedings (2000).

## Biophysical Studies of MARCKS: Implications for Neuroplasticity

Edison, A.S., UF, Biochemistry & Molecular Biology

Bubb, M.R., UF, Medicine

Lenox, R.H., Univ. of Pennsylvania, Psychiatry

Myristoylated alanine-rich protein kinase C substrate (MARCKS) is a prominent protein substrate for protein kinase C that binds calmodulin in a calcium-dependent manner, binds and crosslinks filamentous actin, and is implicated in cellular processes associated with cytoskeletal restructuring, e.g., transmembrane signaling and neurotransmitter release. A highly conserved phosphorylation site domain (PSD) is the binding site for both actin and calmodulin, and may also bind directly to plasma membrane through acidic phospholipids. Considerable work has demonstrated a role for MARCKS in long term events in cell function that are associated with alteration in actin-membrane plasticity in the brain. In particular the regulation of MARCKS expression is involved with brain development, neuronal regeneration, and represents a molecular target in the brain for the action of mood-stabilizers such as lithium in the treatment of manic-depressive illness.

Using NMR spectroscopy, sedimentation, and molecular dynamics simulations, we have documented for the first time conformational changes in the PSD following phosphorylation. These phosphorylation-dependent conformational changes are

correlated with changes in actin crosslinking. In particular, phosphorylated MARCKS-PSD crosslinks actin at significantly higher concentrations than non-phosphorylated MARCKS-PSD. These findings lead to a hypothesis that the actin-MARCKS complex is regulated by specific alterations in conformation of the PSD which changes the availability of actin-binding sites required for crosslinking.

The structural changes are shown in Figure 1. In short, the non-phosphorylated peptide (right) is completely extended in solution while the phosphorylated peptide (left) is compact. This compactness, we hypothesize, leads to substantial changes in the function of MARCKS.

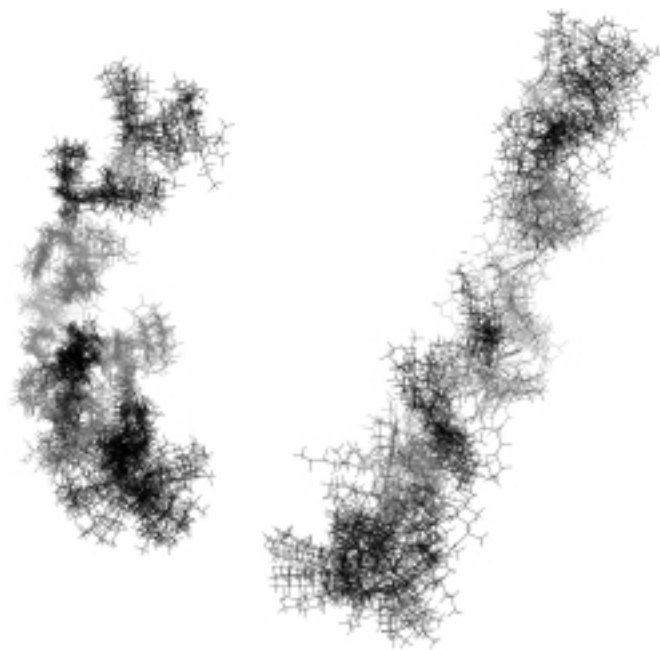


**Figure 1.** Families of structures of MARCKS-PSD with phosphates (red groups on left) and without phosphates. Structures were calculated with molecular dynamics and incorporated NMR data as restraints.

## Structural and Dynamical Studies of IA-3: A Potent Yeast Proteinase A Inhibitor

Edison, A.S., UF, Biochemistry & Molecular Biology

Green, T., UF, Biochemistry & Molecular Biology

Dunn, B., UF, Biochemistry & Molecular Biology

Kay, J., Cardiff Univ., School of Bioscience

Wlodawer, A., National Cancer Institute

Proteases are attractive targets for drug design against microbial pathogens, because the proteases are often essential to the life cycle of the pathogen and are sometimes directly related to acute damage in the host. Moreover, proteases from different species often have slightly different properties, allowing for the development of highly selective inhibitors. This project is focused on elucidating the structural features of a 68 amino acid yeast protein, IA-3, which is a potent inhibitor of yeast proteinase A (YprA).

IA-3 binds to YprA with exceptional affinity ( $K_D$  is sub-nanomolar) and specificity. An x-ray crystal structure of the IA-3/YprA complex has recently been solved in Wlodawer's laboratory (in press, *Nature Structural Biology*), and in that structure IA-3 forms a near-perfect alpha-helix in its first 33 amino acids. The C-terminal domain was not observed in the electron density. Until this finding, all protease inhibitors were thought to bind in extended conformations.

NMR data have been collected on the 33 amino acid N-terminal fragment and full length IA-3 protein. The NMR data, along with CD and biochemical evidence, all support the fact that unbound IA-3 is nearly completely unstructured in solution. This is a surprising finding, given the very tight binding and the near-perfect helix in its interactions with YprA. Using  $^{13}\text{C}/^{15}\text{N}$  labeled IA-3, we are attempting to assign all the resonances of the unfolded IA-3, a difficult task considering that amount of overlap in the spectrum. We have also collect NMR relaxation measurements, which also give strong evidence for an unfolded free state. We will next compare the relaxation properties in the free and bound states to observed differences in dynamics of IA-3. Also, we will begin work to characterize the transition from coil to helix and to examine different mutants for different amounts of helix in solution.

This project is to extend our knowledge of the details of how IA-3 inhibits YprA. With that knowledge, we will be in a strong position to design inhibitors of YprA homologues from pathogenic fungi, such as several species of *Candida*, that have no identified natural inhibitors. These novel inhibitors could prove important in the development of selective new drugs for the control of fungal infections. Moreover, YprA is an aspartic proteinase, so information obtained with YprA/IA-3 interactions may one day lead to new approaches to inhibiting viral aspartic proteinases such as HIV protease.

## Structural Studies of Mutacin 1140

Edison, A.S., UF, Biochemistry & Molecular Biology

Smith, L., UF, Neuroscience

Hillman, J., UF, Oral Biology

Novak, J., Univ. of Alabama, Microbiology and Oral Biology

Mutacin 1140 is a naturally occurring lantibiotic produced by the bacterium *Streptococcus mutans*. Lantibiotics are ribosomally produced antibiotics that contain a large number of post-translational modifications, such as dehydrated amino acids and thioether bridges. The thioether bridges form between cysteine residues and modified serine and threonine residues. Mutacin 1140 has exceptional antibiotic activity against a broad range of Gram-positive bacteria.

The post-translational modifications in lantibiotics make covalent structure determination challenging. Our laboratory has used NMR to determine the complete covalent structure of

mutacin 1140. A manuscript reporting the structure has been submitted for publication. In addition, we have made substantial progress toward solving the three-dimensional structure of mutacin in solution. These studies provide information necessary to study mutacin's mode of action, to engineer novel activities, and to increase the efficiency of its production.



**Figure 1.** Covalent structure of mutacin 1140 determined by NMR, mass spectrometry, and chemical sequencing.

## Structure/Function Relations of Neuropeptides and Neuropeptide Precursor Proteins

Edison, A.S., UF, Biochemistry and Molecular Biology

Zachariah, C., UF, Biochemistry and Molecular Biology

Thomas, S., UF, Biochemistry and Molecular Biology

Espinoza, E., UF, Biochemistry and Molecular Biology

We are using NMR to study the structural properties of a large family of neuropeptides call FMRFamide-like peptides (FLPs). There are several hundred FLPs throughout the animal kingdom, and some organisms have more than 50 different (but closely related) FLPs. Neuropeptides have three main "states" in vivo: (1) They are expressed as longer precursor proteins that often contain multiple copies of peptides. (2) They exist as free, fully processed peptides. (3) They bind to and activate different types of receptors. We are making good progress studying each state.

Recently, we showed that a family of related peptides with single changes in amino acid sequence had large changes in the amount of reverse turn in solution. These changes are inversely correlated with the receptor binding affinity, suggesting that the turns inhibited access of the peptides to the receptor (Edison et al., 1999). The NMR work has now been confirmed computationally with Monte Carlo simulated annealing calculations (Carlacci and Edison, manuscript submitted). We are concluding a study showing structural and biochemical differences in a peptide with two adjacent FLPs separated by a proteolytic processing site. This work is helping us to understand the structural requirements for neuropeptide processing. Finally, we have made significant advances in our attempts to produce the peptide binding domains of one of the FLP receptors.



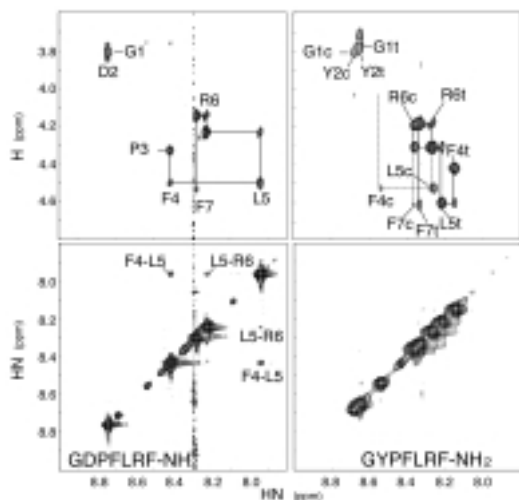


**Figure 1.** NOESY spectra of two closely related FLPs shows large differences, demonstrating that there are large changes in their conformational ensembles in solution.

## EPR and Fluorescence Studies of Myosin Head Structure and Dynamics

Fajer, P., NHMFL/FSU, Biology and Institute of Molecular Biophysics

Adhikari, B., NHMFL/FSU, IMB

Li, H., NHMFL

Sale, K., NHMFL/FSU, Biology

Palm, T., NHMFL

Somerset, J., NHMFL

Brown, L., Univ. of Sydney, Australia, Pathology/NHMFL

Hambly, B., Univ. of Sydney, Australia, Pathology

Muscle is the system of interest in our lab. Muscle is widely regarded as the ultimate biological motor: it transforms the chemical energy of ATP into mechanical work. Just like in a mechanical engine, one can reasonably expect that muscle possesses parts that move when the fuel energy is liberated and mechanical lever arms that impart movement to other structures. Thus the determination of molecular geometry and dynamics is a promising avenue in the elucidation of this basic mechanism. In muscle, force is generated by the cyclic interaction of two proteins, actin and myosin, coupled to the cleavage of ATP. The chemical cycle of myosin ATPase propels a structural cycle of actin-myosin interactions, which include attachment of the myosin motor domain to actin, force generation, filament sliding, and myosin detachment. Taking advantage of the spectral resolution of EPR our approach is to: (a) *determine the reorientation of the chosen domains of the myosin and* (b) *describe their dynamics.*

- *Inter domain mobility of myosin head—EPR.* All the previous EPR work on myosin (including ours) has been done with probes in the catalytic domain. It has been tacitly assumed that the myosin head behaves like a rigid body—movement in the catalytic domain translates into the same movement of the

regulatory domain. Since publication of the crystal structure of the myosin head in 1993, there has been increasing evidence that the crossbridge might not be as rigid as was first assumed. The distal (regulatory) and proximal (catalytic) portions might move independently. Indeed, the interdomain movement was a centerpiece of the hypothesis advanced on the basis of the x-ray structure of the myosin head. We have measured the protein dynamics in these two domains and proven the existence of a hinge separating the regulatory and catalytic domains (Adhikari *et al.*, PNAS, 1997). We have followed up this work with a description of hinge modulators: ionic strength, divalent ions, pH and phosphorylation. We have found that the increase of activity of myosin correlates with the increased mobility of the head. In particular, our work provided support for the hypothesis of a possible mechanism of regulation of smooth muscle – release of the myosin heads from the surface of the myosin filaments.<sup>1</sup>

- *Inter domain mobility: Fluorescence Energy Transfer.* According to a popular hypothesis of muscle contraction, force is generated by a shape change in the myosin head crossbridge driven by the hydrolysis of ATP. In particular, the jackknifing movement of the catalytic domain with respect to the regulatory domain is thought to generate the mechanical strain between connected actin and myosin filaments. One way to observe the shape changes in a molecule is to measure distances between selected sites before and after the shape change occurs. We utilized a fluorescence energy transfer technique as a molecular ruler and triangulated distances between the distal and proximal domains of the myosin head. The distance measurements combined with the extensive molecular modeling revealed that: (a) the distance changes are consistent with the *jackknifing* shape change of the myosin head, such a change accounts for the 8 nm axial movement of the tip of myosin head which correlates well with the size of force generating step (Figure 1); (b) that the actin-distal regulatory domain behaves like a



**Figure 1.** Movement of the tail of myosin head consistent with FRET/LRET observed changes using Cohen's crystal structure as a model for a prepower stroke state.

rigid body—plays a role of a passive force lever amplifying the torque generated in the catalytic domain.<sup>2</sup>

Acknowledgements: This work was supported by NSF, the American Heart Association, and the NHMFL.

<sup>1</sup> Adhikari, B., *et al.*, *Biochemistry*, **38**:2127-2132 (1999).

<sup>2</sup> Palm, T., *et al.*, *Biochemistry*, **38**, 13026-13034 (1999).

## Gas-Phase Bovine Ubiquitin Cation Charge State Conformations Resolved by Gas-Phase Hydrogen/Deuterium Exchange Rate and Extent

Freitas, M.A., NHMFL

Hendrickson, C.L., NHMFL

Emmett, M.R., NHMFL

Marshall, A.G., NHMFL/FSU, Chemistry

The gas-phase hydrogen/deuterium exchange of  $[M + nH]^{n+}$  ( $n = 5-13$ ) ions of bovine ubiquitin with the H/D exchange reagent  $D_2O$  are examined by electrospray ionization FT-ICR mass spectrometry. Different gas-phase protein conformations could be resolved according to difference in extent of H/D exchange. The 5+ and 6+ charge states display broad distributions of conformations ranging from 0-80% deuterium incorporation. In contrast, each of the higher charge states, 7-11+ and 13+, displays a single major isotopic distribution, whereas the 12+ charge state separates into two isotopic distributions of comparable abundance (see figure). In general, H/D exchange rates decrease with increasing charge state. At 9.4 T, it is possible to trap a large number of ions for a long reaction period (up to 1 h) at relatively high pressure ( $2 \times 10^{-7}$  torr). These results demonstrate the capability of FT-ICR mass analysis following gaseous H/D exchange of electrosprayed proteins to disperse different gas-phase protein conformations for subsequent isolation and characterization.

Acknowledgements: The authors thank David Clemmer (Indiana University, Bloomington Indiana) for helpful discussions and for providing his unpublished data. This work was supported by the NSF (CHE-94-13008, CHE-93-22824) National High Field FT-ICR Facility, Florida State University, and the NHMFL at Tallahassee, Florida.

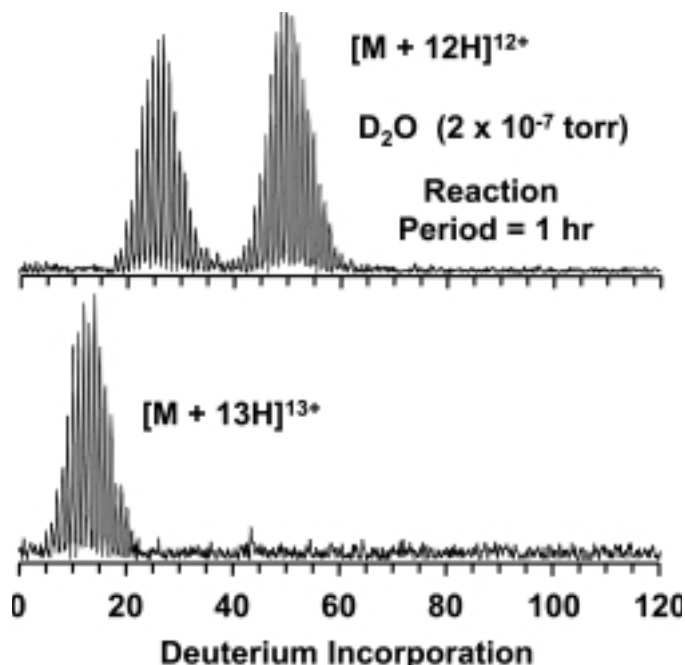


**Figure 1.** H/D exchange of isolated charge states of ubiquitin. Upper panel: 12+ charge state (2 conformations). Lower panel: 13+ charge state (1 conformation).

<sup>1</sup> Freitas, M.A., *et al.*, *Int. J. Mass Spectrom.*, **185/186/187**, 565-575 (1999).

<sup>2</sup> Marshall, A.G., *et al.*, *Mass Spectrometry in Biology and Medicine*, Ed. A.L. Burlingame and S.A. Carr (Humana Press, Totowa, NJ, 1999), 31-52.

## Membrane Protein Structure as Determined by Use of $^{19}F$ Solid State NMR Spectroscopy **IHRP**

Gao, F., Univ. of California at Los Angeles, Physiology, and Howard Hughes Medical Institute (HHMI)

Fu, R., NHMFL

Wang, J., NHMFL

Cross, T.A., NHMFL/FSU, Chemistry

Kaback, H.R., UCLA, HHMI

Solid state NMR is now being applied in biological systems, especially with integral membrane proteins.<sup>1</sup> Wild-type and genetically engineered proteins can be investigated and detailed information about side chains, ligands, and binding sites can be deduced. The low sensitivity of  $^{13}C$ ,  $^{15}N$ , and  $^2H$ , however, presents a considerable problem in terms of the availability of the protein, sample volume, and measurement time.  $^{19}F$  is the most sensitive NMR nucleus besides  $^1H$  and  $^3H$ . Since there is no background signal from a protein,  $^{19}F$  can be specifically introduced into protein using site-directed chemical labeling for a unique probe. The dipolar coupling between two  $^{19}F$  is much greater than that of  $^{13}C$ ,  $^{15}N$  pairs, thus allowing

for characterization of long distance constraint (up to 15 Å), which has significant advantages in protein structural mapping. Although,  $^{19}\text{F}$  is ideally suited to carry out highly sensitive measurements of intranuclear distances and angles and has been widely used in solution NMR, it has not been applied to oriented samples in solid state NMR.

In the past year, we have explored the possibility of using  $^{19}\text{F}$  solid state NMR to obtain structural information of the lactose permease. A library of unique permease mutants containing single-Cys residues at every position in lac permease was previously constructed in Dr. Kaback's lab. The expediency of the manipulations, as well as the ability to insert a Cys residue at any positions in the protein, is greatly facilitated by the availability of a cassette lacY gene (EMBL X-56095) that contains a unique restriction site approximately every 100 base pairs. There are 6 irreplaceable residues in the *E. coli* lac permease. They are 126E, 144R, 269E, 302R, 322H and 325E. According to the current proposed model, the spatial relationships of these residues are critical for coupling between the protein electrochemical gradient and the substrate translocation. It has been shown in the previous studies that Glu325 and Arg302 are in close proximity. The double-Cys permease mutant R302C/E325C was constructed in functional lac permease devoid of native Cys residues. Proteins were purified, labeled with the thiol specific reagent, p-fluorobenzeneethiol, and reconstituted into proteolipsomes. Well oriented samples were prepared, and  $^{19}\text{F}$  signals were detected with a Bruker DMX 300 MHz NMR spectrometer using less than 3 mg of protein. Dipolar coupling of  $^{19}\text{F}$  between these two positions was observed, indicating that residue 302 and 325 are in close proximity. The result is in good agreement with results from site-directed excimer fluorescence. Several double Cys mutants have been constructed. They are 126C/144C, 269C/322C, 269C/325C, 269C/302C, 126C/269C, and 144C/269C. Distances between these residues will be determined on the 833 MHz spectrometer.

Results of this collaborative research have laid the foundation for further refining the helical packing model and substrate binding site of lactose permease using  $^{19}\text{F}$  solid state NMR. It is anticipated that further collaboration will not only provide more insight into the structure and function of this enzyme system and the transport mechanism in general, but will also expand the emerging methodology of  $^{19}\text{F}$  solid state NMR for the study of other membrane proteins.

<sup>1</sup> Cross, T.A., Ann. Report on NMR Spectroscopy, 29, 123 (1994).

## Behavioral and Neural Effects of Static High Magnetic Fields

Houpt, T.A., FSU, Biological Science

Smith, J.C., FSU, Psychology

Snyder, D., FSU, Neuroscience

Jahng, J.W., Yonsei College of Medicine, Korea,  
Pharmacology

Advances in magnetic resonance imaging (MRI) are driving the development of faster and higher resolution MRI machines. Little is known about the sensory or physiological effects of static magnetic fields of high strength on mammals and humans. We have recently discovered that 30 min exposure to a 9.4 T magnetic field has behavioral and neural effects on rat. At the behavioral level, magnetic field exposure induced a conditioned taste aversion (CTA) after pairing with the taste of saccharin. Because CTA has proven to be a sensitive index of visceral malaise, this suggests that the magnetic field may be an aversive stimulus to the rat.

At the neural level, the same exposure induced specific and significant c-Fos immunoreactivity, a marker of neuronal activation, in the rat brainstem. Magnet-exposed rats (n=6) were confined in a Plexiglas tube for 30 min within the 9.4 T magnet. Sham-exposed rats (n=6) were restricted in the same manner for the 30-min period, but not exposed to the magnetic field. One hour later, rats were overdosed with sodium pentobarbital, and transcardially perfused. Brain sections through the medulla and pons were processed for c-Fos. The number of c-Fos-positive cells was quantified in several visceral and stress relays (e.g. nucleus of the solitary tract (NTS), locus ceruleus (LC) and parabrachial nucleus (PBN) and in vestibular nuclei (e.g. the medial vestibular nucleus (MeV), prepositus (Prp), and supragenualis (SG); see Figure 1).

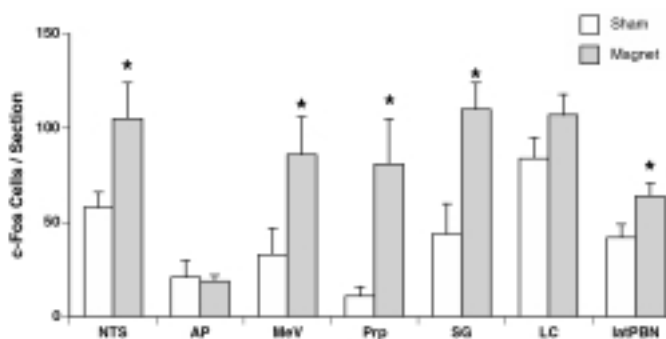


**Figure 1.** Exposure to a 9.4 T magnetic field activated neurons in regions of the rat brain sensitive to vestibular and visceral stimulation, as indicated by increased numbers of c-Fos-expressing compared to sham-exposed rats.

Both the behavioral response and the pattern of c-Fos activation are similar to the effects of vestibular disturbance, such as rotation and motion sickness. Therefore, our working hypothesis is that the magnetic field activates the vestibular apparatus of



the inner ear, causing vertigo and CTA acquisition. This is consistent with the self-reports of vertigo and nausea in humans exposed to 4 T magnetic fields. These preliminary findings suggest that CTA and c-Fos expression can be used in an animal model of the behavioral and neural effects of high-strength, static magnetic fields.

## Development of Prostate MRI/S Using Transceive Coils at 3 T

Kim, H.W., Univ. of Florida Brain Institute (UFBI)/UF, Radiology

Buckley, D.L., UFBI/UF, Neuroscience

Peterson, D., UFBI/UF, Radiology

Duensing, R., UFBI/UF, Radiology

Narayan, P., UF, Neuroscience

Blackband, S.J., UFBI/UF Center for Structural Biology/UF, Neuroscience/NHMFL

MR studies of the human prostate have so far been limited to 1.5 T or below. Like most applications of MR, however, higher field strengths offer the potential of increased SNR and spectral dispersion. Although field strengths above 1.5 T are now available for human studies, the rf technology has not been developed to take advantage of these potential increases (most 3 T (and above) scanners do not have body coils—the effort has been on neurological studies). Further, the rf coil design becomes more difficult with increasing frequency making the design problematic.

A major problem as the frequency increases is the increased rf power that is required, making large (body) rf coils difficult to construct. To alleviate this problem, researchers at UF have developed phased array transceive rf coils.<sup>1</sup> In this work, we constructed a transceive phased array pelvic coil suitable for MR studies of the human prostate. A coil was constructed of 4 phased array pelvic coils operating at 3 T (128 MHz). Using the coil, the first MR images (see images below) and spatially localized <sup>1</sup>H spectra of the human prostate were obtained at 3 T. The spectra clearly show increased spectral dispersion and give an SNR comparable to that obtained using an endorectal coil at 1.5 T. In particular the citrate quadruplet is demonstrated for what we believe is the first time. Potentially, the 3 T would

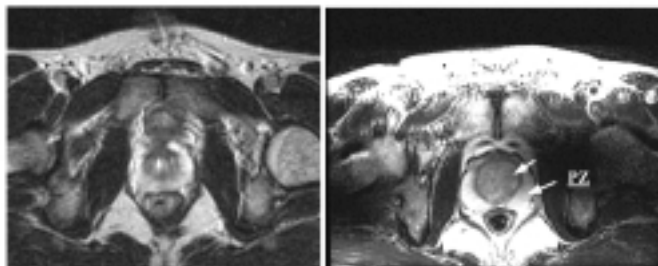


Figure 1. Left: 1.5 T prostate image; right: the first 3 T prostate image.

be very useful when the endorectal coil is contraindicated. This work has been presented at a meeting<sup>1</sup> and has been submitted for publication.

Acknowledgements: This work was supported by NIH and UFBI.

<sup>1</sup> Kim, H.W., *et al.*, International Society for Magnetic Resonance in Medicine 7<sup>th</sup> Annual Meeting, Philadelphia, May (1999).

## Identification of Intact Proteins in Mixtures by Alternated Capillary Liquid Chromatography Electrospray Ionization and LC-ESI Infrared Multiphoton Dissociation Fourier Transform Ion Cyclotron Resonance Mass Spectrometry

Li, W., FSU, Chemistry

Hendrickson, C.L., NHMFL

Emmett, M.R., NHMFL

Marshall, A.G., NHMFL/FSU, Chemistry

In 1999, we presented a novel method for rapidly identifying proteins in complex mixtures. A list of candidate proteins (including provision for post-translational modifications) is obtained by database searching, within a specified mass range about the accurately measured mass (e.g.,  $\pm 0.1$  Da at 10 kDa) of the intact protein, by capillary liquid chromatography electrospray ionization Fourier transform ion cyclotron resonance mass spectrometry (LC ESI FT-ICR MS). On alternate scans, LC ESI infrared multiphoton dissociation (IRMPD) FT-ICR MS yields mostly b- and y-fragment ions for each protein, from which the correct candidate is identified as the one with the highest “hit” score (i.e., most b- and y-fragments matching the candidate database protein amino acid sequence masses) and sequence “tag” score (based on a series of fragment sequences differing in mass by 1 or 2 amino acids). The method succeeded in uniquely identifying each of a mixture of five proteins treated as unknowns (melittin, ubiquitin, GroES, myoglobin, carbonic anhydrase II), from more than 1,000 possible database candidates within a  $\pm 500$  Da mass window.

Acknowledgements: We thank John P. Quinn for maintaining the high-performance 9.4 T FT-ICR instrument. This work was supported by NSF (CHE-94-13008), NIH (GM-31683), Florida State University, and the NHMFL in Tallahassee, FL.

<sup>1</sup> Li, W., *et al.*, *Anal. Chem.*, **71**, 4397-4402 (1999).



## Intracellular Mobility of Solute Compounds in Striated Muscle

Moerland, T.S., FSU, Biological Sciences  
 Vanderlinde, O.H., FSU, Biological Sciences  
 Carbone, F.A., FSU, Biological Sciences

This project employs pulsed-field gradient  $^{31}\text{P}$  NMR to investigate the mobility of small solutes and metabolite compounds in living cells of striated muscle. The goal is to attain a better understanding of the effects of cellular ultrastructure on the intracellular diffusive mobility of small solute molecules, including the phosphorylated compounds that are important to energy metabolism. Experiments utilize the wide-bore 600 MHz Bruker DMX NMR spectrometer at the NHMFL. Because of its singular combination of sensitivity and wide bore, this system is uniquely suited for analysis of physiological transients in living tissue.

Experiments show that intracellular diffusion is highly anisotropic in several different types of striated muscle. Diffusion of phosphagen metabolites in muscle from mouse, lobster, and fish is similar in that diffusion across the radius of the cylindrically shaped muscle cells restricted far more than diffusion along the long axis. Although the phenomenon is similar in these different muscle types, there are quantitative differences in the degree of anisotropy. These differences are correlated with characteristic differences between muscles in cellular ultrastructure. These results show that anisotropy in diffusion is a general property of solute mobility in striated muscles, and that the most likely determinants of this anisotropy are features of the intracellular architecture.

Acknowledgement: This work is supported by NSF IBN-98-08120.

## Stress Response to High Magnetic Fields in Transgenic Arabidopsis Plants **IHRP**

Morgan, A.N., UF, Physics  
 Watson, B.C., UF, Physics  
 Maloney, J.R., UF, Physics  
 Meisel, M.W., UF, Physics  
 Brooks, J.S., NHMFL/FSU, Physics  
 Paul, A.-L., UF, Horticultural Sciences  
 Ferl, R.J., UF, Horticultural Sciences

With increasingly greater strength magnetic fields becoming available in research and medicine, the response of living tissue exposed to high magnetic fields has come under investigation. In preliminary work,<sup>1</sup> we observed a stress response in transgenic arabidopsis (*Arabidopsis thaliana*) plants when the specimens were exposed to homogeneous magnetic fields of 18.9 T for 2.3 hours. To clarify this result, genetically engineered arabidopsis

plants were exposed to homogeneous magnetic fields of varying strengths using a superconducting NMR magnet (0 to 9 T) at UF and a resistive magnet (0 to 25 T) at the NHMFL-Tallahassee. The engineered plants produce the enzyme  $\beta$ -glucuronidase (GUS) when under stressful environmental conditions. The level of GUS activity is determined through qualitative histochemical and quantitative fluorometric assays. The control group of plants experienced baseline levels of GUS activity, but some of the plants that were exposed to magnetic fields in excess of 17 T show increased stress response. Additional work is being pursued to clarify this response by quantitatively mapping the stress response as functions of magnetic field strength and exposure times. Further details about this aspect of the research program and our study of the magnetic levitation of these plants is available elsewhere.<sup>2</sup>

<sup>1</sup> Stalcup, T.F., *et al.*, in *Physical Phenomena in High Magnetic Fields -III (PPHMF-III)*, eds. Z. Fisk, L. Gor'kov, R. Schrieffer (World-Scientific, Singapore, 1999) pp. 659-662.

<sup>2</sup> <http://www.phys.ufl.edu/~meisel/maglev.htm>

## Determination of 3D Helix Bundle Structure of Influenza Virus M2-TMP Based on Solid State NMR Distance Measurement

Nishimura, K., NHMFL  
 Kim, S., NHMFL/FSU, Institute of Molecular Biophysics  
 Cross, T.A., NHMFL/FSU Chemistry, and Institute of Molecular Biophysics

Influenza A viral M2 protein has ion channel function by forming of a helix bundle of four transmembrane helices. Thus, it is essential to determine the three dimensional structure of this helical bundle incorporated into lipid bilayers to reveal the mechanism of channel function. In the previous work, the monomeric transmembrane helix structure was determined,<sup>1</sup> and a tetramer packing motif was modeled.<sup>2</sup>

Here we tried to characterize the helix bundle structure in a lipid bilayer by measuring the interhelical  $\text{His}^{15}\text{N}_\pi$   $^{37}\text{Trp}^{41}$  [ $^{13}\text{C}_\gamma$ ] side chain distance. M2-TMP (Ser<sup>22</sup>-Leu<sup>46</sup>) was synthesized by solid phase method using a peptide synthesizer. Unoriented 50% hydrated (by total sample dry weight) samples at pH 5 were prepared by a procedure reported previously<sup>1</sup>. REDOR (Rotational Echo Double Resonance) spectroscopy was applied to determine the  $^{13}\text{C}$ - $^{15}\text{N}$  heteronuclear dipolar interaction. Experiments have been performed under the XY-8 compensation pulse sequence as  $^{13}\text{C}$ -observation under the MAS 4 KHz  $\pm$  3 Hz, at a temperature of 32°. The sample was packed within 5.4 mm in the central position of sample tube to keep rf homogeneity. A relatively strong signal was observed at 156 ppm Observed  $^{13}\text{C}$ - $^{15}\text{N}$  heteronuclear dipolar interaction was determined to be 20 Hz  $\pm$  5 Hz which is greater than predicted for the intramolecular interaction, which is obtained based on single transmembrane structure.<sup>1</sup> In the lipid bilayer

environment, the observed heteronuclear dipolar interaction is affected by both the interatomic distance and angle between  $^{13}\text{C}$ - $^{15}\text{N}$  dipolar vector and bilayer normal axis, because of the presence of global motion of the helix bundle about the bilayer normal. The intramolecular side chain distance must be longer than  $6.1\text{\AA}$  and by taking into account of the global molecular motion, the intramolecular dipolar interaction would be impossible to detect. Consequently, the parameter pairs for distance and angle were obtained to restrict structure configuration between helices as shown in Figure 1 based on an intermolecular distance. This information will give us a helix bundle structure in the lipid bilayer environment.

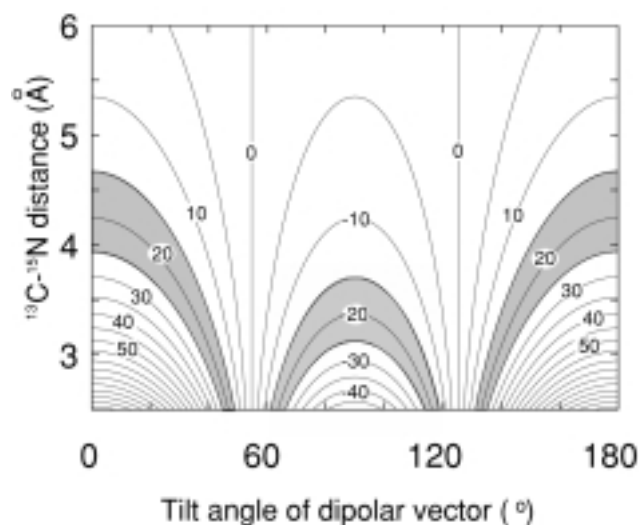


**Figure 1.** The correlation map for the parameter pair of  $^{13}\text{C}$ - $^{15}\text{N}$  distance and angle between the bilayer normal and dipolar vector. The possible area to give dipolar interaction  $20 \pm 5$  Hz is colored by gray.

<sup>1</sup> Kovacs, F., *et al.*, *Biophys. J.*, **73**, 2511 (1997).

<sup>2</sup> Salomon, D., *et al.*, *Biophys. J.*, **76**, A123 (1999).

## ENDOR on Short-Lived Carotenoid Triplet States of the Outer Antenna Complex PCP of Dinoflagellates

Parrish, S., UF, Chemistry

Angerhofer, A., UF, Chemistry

Carotenoids play an important role in the lives of plants and photosynthetic bacteria. On the one hand they act as additional antenna pigments, harvesting the light in the blue and green spectral region where the chlorophylls absorb only weakly. On the other hand they are essential for their photoprotective function, quenching any chlorophyll triplet states that might be excited by excess light irradiation. Thus they efficiently prevent singlet oxygen sensitization that would cause oxidative damage and breakdown of the photosynthetic cell components. The outer antenna complex of dinoflagellates consists of a monomer or dimer (depending on the organism) of a pigment-protein complex containing 1 chlorophyll *a* molecule and 4 peridinin carotenoids in close proximity. In isolated form, the chlorophylls,

once excited, cannot transfer their energy on to other antenna complexes and de-excitation mainly proceeds through intersystem crossing and triplet formation. Thus, the photoprotective role of the peridinin molecules can be studied in such isolated antenna preparations. The lifetime of the chlorophyll triplet state that is generated from a singlet excitation within a few ns is very short, of the order of 20 to 30 ns, and depends little on temperature. Within this time a triplet state is formed on one of the circumferential peridins and decays through radiationless ISC channels with a lifetime of 25  $\mu\text{s}$ . This high relaxation rate leaves very little time to perform an ENDOR experiment and gather information about the anisotropic hyperfine structure which may yield information on the structure of the triplet-carrying molecule.

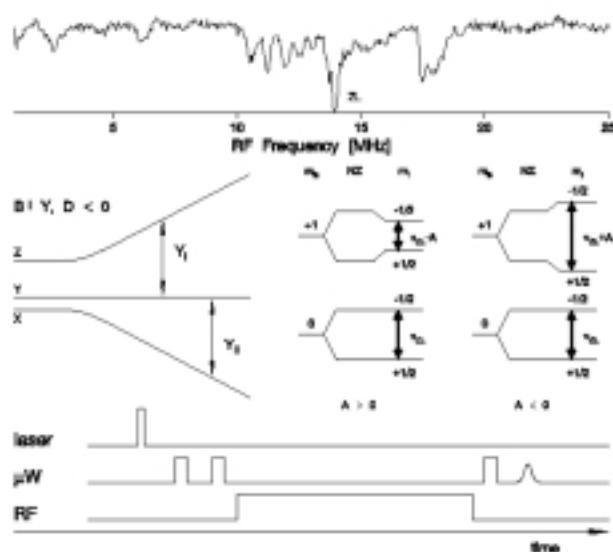


**Figure 1.** Top: Mims-ENDOR spectrum of the peridinin triplet state in PCP at 100 K taken on the  $Y_1$ -peak at 3282 G and  $\nu = 9.7121$  GHz. Middle: Energy level diagrams explaining the ESR transitions (left) when  $B \parallel Y$  and  $D < 0$ , and the ENDOR transitions for positive (middle) and negative (right) hyperfine coupling constants (hfc).  $D < 0$  for polyenes and the zero field level ordering has been chosen accordingly. For  $B \parallel Y$  the protons with positive hfc therefore show up on the low frequency side of the zero matrix line (ZL, Larmor frequency of free protons at the given field), while the ones with negative hfc show up on the high frequency side. Bottom: Pulse sequence of the Mims-ENDOR experiment used. Duration of the laser pulse was approximately 4 ns. The duration of the three microwave pulses was 16 ns, the RF pulse 6  $\mu\text{s}$ . The time delay between laser and first microwave pulse was 200 ns,  $\tau$  between the first two microwave pulses was 112 ns which is also the distance between the third microwave pulse and the resulting stimulated echo. The time  $T$  between the second and third microwave pulse was 6.5  $\mu\text{s}$  to accommodate the RF pulse.

Here we report for the first time a successful time-resolved MIMS ENDOR experiment taken after an initial laser pulse of 4 ns duration to generate the triplet states (see Figure 1). It shows a range of proton signals with positive hyperfine coupling constants (hfc) on the low frequency side. Triplet ENDOR spectra are inherently asymmetric unlike their counterparts of spin-1/2 species. The reason for this is that the  $T_0$  electron spin level does not exert a hyperfine field on the nuclei (see also the energy diagram in Figure 1 for further explanation). This leads

to a strong zero line (ZL) at the nuclear Larmor frequency. While a detailed assignment is not possible at this point and will require the measurement of the full orientation dependence that is possible by the inherent orientational selection of the triplet ESR powder spectrum, comparison with calculations on  $\beta$ -carotene where the succession of the protons along the polyene chain gives rise to step-wise decreasing hfc's show good agreement with our spectrum. These calculations show relatively large negative hfc's between  $-5$  and  $-7$  MHz for protons 11, 11', and 15, 15' on the chain. A similar situation may be expected for peridinin although it is of course asymmetric and therefore the assignment of the protons is still unclear. Finally, large positive hfc's of up to 15 MHz have been predicted for the methyl protons in  $\beta$ -carotene and a similar situation may well be responsible for the weak peaks around 6 and 2.6 MHz in the peridinin ENDOR spectrum.

## Helix Bundles and Coiled Proteins

Quine, J.R., FSU, Mathematics/NHMFL

Denny, J.K., FSU, Mathematics/NHMFL

Global structural information about the M2 transmembrane (M2-TMP) peptide from influenza A from PISEMA data obtained by T. A. Cross's group indicates that this peptide forms a four-helix bundle.<sup>1</sup> We give an initial approximation to the structure by defining a model bundle of straight helices with  $C_4$  symmetry characterized by four parameters.

This approach models each helix in the bundle using only the axis of the helix, which is depicted (Figure 1) as an oriented line segment  $l$  (on a line  $L$ ) of length  $\lambda$ . The position of  $l$  with respect to the symmetry axis of the bundle is determined by three other parameters,  $\delta$ ,  $\tau$ , and  $\gamma$ . The tilt angle between  $l$  and the axis  $a$  of the bundle (also the bilayer normal) is denoted  $\tau$ . The distance of segment  $l$  from the bundle axis  $a$  is denoted  $\delta$ . The position of the initial point of  $l$  on this line  $L$  with respect to the point on  $L$  that is closest to the axis  $a$  is denoted  $\gamma$ . These four parameters,  $\tau$ ,  $\lambda$ ,  $\delta$ , and  $\gamma$ , uniquely determine the position of the axis of one helix in the bundle. Next, a left-handed, four-helix bundle with  $C_4$  symmetry is generated by repeated application of a  $90^\circ$  rotation about the bundle axis to one modeled helix axis.

The geometry of this model yields several formulas for key angles in the bundle. The crossing angle  $\omega$  of two adjacent helix axes is related to the tilt angle  $\tau$  by  $\omega = \arccos(\cos^2\tau)$ . Also, the smallest distance  $d$  between two adjacent helix axes can be expressed in terms of the above parameters by

$$d = \frac{2\delta \cos \tau}{\sqrt{1 + \cos^2 \tau}}.$$

Thus, the crossing angle and packing radius depend only on the tilt  $\tau$  and the distance  $\delta$  of the helix axes from the bundle axis. The problem in M2-TMP structure determination is to compute these parameters from solid-state NMR data and to determine

another parameter,  $\rho$ , that describes the position of the protein helix on its axis.

The next problem is to refine the straight helix model and determine the degree of coiling. The phenomenon of coiling in coiled or bundled helical proteins is caused by the equilibrium between the forces of hydrogen bonding whose optimization requires 3.6 residues per turn, and the forces of van der Waals interactions among the helices in the bundle. Finding sets of torsion angles for a protein backbone that produce a particular coiled structure is the most general case of the local conformational deformation problem defined by Go and Sheraga<sup>3</sup>; however, the large number of parameters involved make the problem computationally difficult. Current efforts focus on developing a method based on the discrete Frenet frame and Crick's equation for a coiled coil<sup>2</sup> that will significantly reduce the number of parameters in the problem.

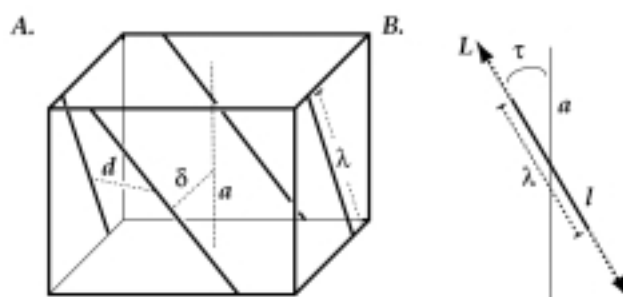


**Figure 1.** Axes of four helices in a bundle and associated parameters.

<sup>1</sup> Kovacs, F.A., *et al.*, *Biophys. J.*, **74**, 2511 (1997).

<sup>2</sup> Crick, F.H.C., *Acta Cryst.*, **6**, 689 (1953).

<sup>3</sup> Go, N., *Macromolecules*, **3**, 178 (1970).

## The Primary Electron Donor of Photosystem I: A High-Field EPR Analysis of Mutants with Altered Axial Ligands

Redding, K.E., Univ. of Alabama, Chemistry and Biochemistry

Boudreaux, B.G., Univ. of Alabama, Chemistry and Biochemistry

MacMillan, F., Goethe Univ. of Frankfurt, Chemistry

Maniero, A.-L., NHMFL

Brunel, L.-C., NHMFL

The Photosystem I (PSI) complex catalyses the transfer of an electron across the thylakoid membrane from plastocyanin to ferredoxin, using the energy of an absorbed photon. The initial photochemical event is the transfer of an electron from the excited state of  $P_{700}$ , a pair of chlorophylls serving as the primary electron donor, to a single chlorophyll serving as the primary acceptor. In order to identify the axial ligands to the chlorophylls of  $P_{700}$ , we had performed a systematic survey of

conserved histidines in the last 6 transmembrane segments of the related polytopic membrane proteins, PsaA and PsaB, which together form the core of PS1. After spectroscopic analysis of the  $P_{700}$  (visible, infrared, and EPR), we found that only mutation of histidines in helix 10 affected  $P_{700}$  in any significant way.<sup>1</sup> Our conclusion was that these histidines were most likely serving as the axial ligands to the chlorophylls of  $P_{700}$ . Our earlier EPR analysis at 9.5 GHz, however, was only able to detect changes in hyperfine interactions; we were not able to observe directly changes in the g tensor of the oxidized primary donor ( $P_{700}^+$ ). In this study, we examined mutants that change the putative ligands from histidine to glutamine on both the PsaA side and PsaB side, as well as a double mutant that contains both mutations.

The  $P_{700}^+$  cation radical was generated by illumination of thylakoid membranes in the presence of ferricyanide immediately before and during freezing in liquid nitrogen. EPR spectra were recorded at 330 GHz and 5-10 K; a P/Si standard was used to determine the actual magnetic field experienced by the sample. Spectra are shown in Figure 1. As can be seen, the g tensor is completely resolved in each preparation. It is also apparent that mutation of either histidine perturbs the  $P_{700}^+$  g tensor. Calculated g-values are tabulated in Table 1. There are obvious differences induced by the mutations, and these are probably due to the differences in geometry of the spin distribution over the two halves of the chlorophyll dimer. A quantitative explanation of these effects awaits simulation of the spectra, which is currently in progress. We tentatively assign these effects to subtle changes in the geometry of the  $P_{700}$  dimer caused by the conversion of the axial ligand to glutamine. Such changes in the axial ligands to the primary donor of the purple bacterial reaction center allowed incorporation of bacteriochlorophylls at those sites, and subtle perturbations were also observed in that case.<sup>2</sup> Mutation of these to leucine,

however, caused replacement of bacteriochlorophyll with bacteriopheophytin (i.e., loss of the central  $Mg^{2+}$ ).<sup>2</sup> Interestingly, by low-field<sup>1</sup> or high-field (data not shown), the EPR spectrum of the PsaB-H656L mutant is much more drastically perturbed.

**Table 1.** Calculated g values.

	WT	PsaA-H676Q	PsaB-H656Q	double e mutant
<b>g<sub>xx</sub></b>	2.00311	2.00309	2.00307	2.00305
<b>g<sub>yy</sub></b>	2.00270	2.00264	2.00269	2.00272
<b>g<sub>zz</sub></b>	2.00228	2.00231	2.00213	2.00221

<sup>1</sup> Redding, K., *et al.*, EMBO J., **17**, 50-60 (1998).

<sup>2</sup> Bylina, E. J.; *et al.*, Biochemistry, **29**, 6203-10 (1990). Bylina, E. and Youvan, D., Proc. Natl. Acad. Sci. USA, **85**, 7226-7230 (1988).

## Structural Validation of Saccharomicins by High-Resolution and High Mass Accuracy Fourier Transform Ion Cyclotron Resonance Mass Spectrometry and Infrared Multiphoton Dissociation MS/MS

Shi, S.D.-H., FSU, Chemistry  
Hendrickson, C.L., NHMFL  
Marshall, A.G., NHMFL/FSU, Chemistry  
Siegel, M.M., Wyeth-Ayerst Research  
Kong, F., Wyeth-Ayerst Research  
Carter, G.T., Wyeth-Ayerst Research

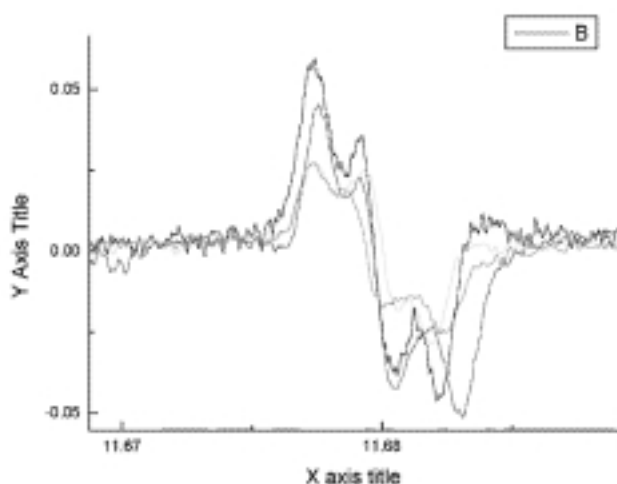


**Figure 1.** EPR spectra of different  $P_{700}^+$  preparations (see text and Table).

Exceptionally high mass resolving power and mass accuracy, combined with  $MS^n$  capability make Fourier transform ion cyclotron resonance (FT-ICR) mass spectrometry a powerful tool for structure verification and determination of biological macromolecules. By means of local internal calibration and electron mass correction, mass accuracy better than  $\pm 0.5$  ppm was achieved for two oligosaccharide antibiotics, Saccharomicins A and B, consistent with the proposed elemental compositions based upon NMR data. High resolution and high mass accuracy MS/MS data were obtained for both oligosaccharides by use of infrared multiphoton dissociation (IRMPD) with a 40 W continuous-wave  $CO_2$  laser. The spectra were charge-state deconvolved by the "Z-Score" algorithm to yield much simpler mass-only spectra. Sequences of 15 sugar residues could be confirmed from the charge state deconvolved accurate mass MS/MS spectra for Saccharomicins A (see figure) and B, even without use of traditional prior permethylation.

**Acknowledgements:** The authors thank Forest M. White, Catherine E. Costello, and Bruce B. Reinhold for helpful discussions. This work was supported by Wyeth-Ayerst Research, and by grants from the NSF National High Field



FT-ICR Mass Spectrometry Facility (CHE-94-13008), Florida State University, and the National High Magnetic Field Laboratory in Tallahassee, FL.

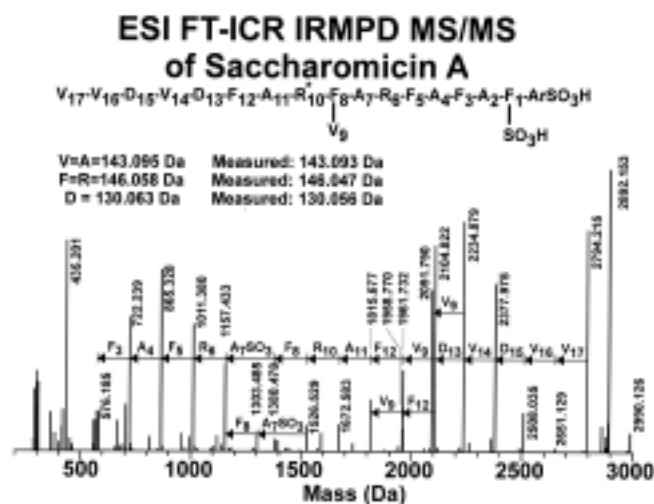


Figure 1. ESI FT-ICR IRMPD MS/MS of Saccharomicin A.

<sup>1</sup> Shi, S.D.-H., *et al.*, J. Am. Soc. Mass Spectrom., **10**, 1285-1290 (1999).

## NMR Studies of *In Vitro* and *In Vivo* Spinal Cords

Silver, X., UF, Biochemistry  
 Inglis, B.A., Univ. of Florida Brain Institute (UFBI)/UF  
 Wirth, E.D., UFBI/UF, Neuroscience  
 Anderson, D.K., UF, Neuroscience  
 Bossart, E.L., UF, Physics  
 Reier, P.J., UFBI, UF, Neuroscience  
 Mareci, T.H., UFBI/UF, Biochemistry/NHMFL

The evaluation of the utility of MR studies in the assessment and monitoring of the spinal cord after injury and during repair in animal models remains a major focus of the MR group at UF. This project has required the development of several technical aspects of MR, as well as technique and data processing developments, and continues in support of studies on the effectiveness of tissue transplantation as a means of repairing spinal cords.

Over the last couple of years we have developed novel inductively coupled implantable rf coils for examination of the spinal cord *in vivo*, and have obtained the first <sup>31</sup>P spectra using implanted coils.<sup>1</sup> In addition, we are now developing phased array external coils to complement these implanted coils. We have also recently demonstrated that the water diffusion coefficient in the spinal cord tissue is at least biexponential and for the moment assume (like others) that this represents intra and extracellular compartments.<sup>2</sup> We have also developed diffusion tensor imaging of the spinal cord and recently used

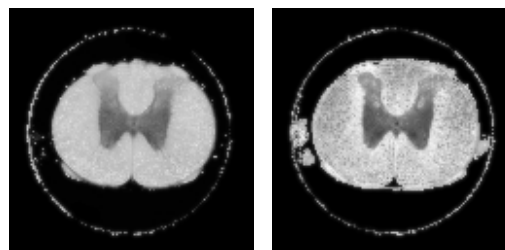


Figure 1. Diffusion tensor images of the fast (left) and slow(right) diffusing water components in an excised spinal cord.

the technique to evaluate tumor morphology in the spinal cord.<sup>3</sup> Combining the biexponential information with the tensor techniques, we have also generated the first biexponential diffusion tensor images of the excised spinal cord (see Figure 1 for example). More recently we have obtained the first biexponential diffusion maps in a rat spinal cord *in vivo*, illustrating the exciting potential of getting at least a limited form of this kind of information *in vivo* on humans.

Acknowledgements: This work was supported by NIH, the State of Florida, and the Brain and Spinal Cord Injury Research Trust Fund.

- <sup>1</sup> Silver, *et al.*, ISMRM 7th Annual Meeting, (1999).  
<sup>2</sup> Bossart, *et al.*, ISMRM 7th Annual Meeting, (1999).  
<sup>3</sup> Inglis, *et al.*, AJNR 20:713-716 (1999).

## Electronic Relaxation of NMR Gd(III) Contrast Agents at High Magnetic Fields

Smirnova, T.I., Univ. of Illinois, Illinois EPR Research Center (IERC)  
 Smirnov, A.I., Univ. of Illinois, College of Med., IERC  
 Belford, R.L., Univ. of Illinois, Chemistry, Medicine, Information Sciences, IERC  
 Clarkson, R.B., Univ. of Illinois, Medicine and Veterinary Clinical Medicine, IERC  
 Van Tol, J., NHMFL

Gadolinium (III) complexes are widely used in medicine as paramagnetic contrast agents (PCAs) for Magnetic Resonance Imaging (MRI). Many parameters contribute to the relaxivity of the complex. Characteristics of interest are electronic relaxation times, magnitude, and correlation time of the zero field splitting, rotational correlation time of the complex, number of water molecules in the complex inner sphere, and the rate of their exchange with the bulk water. Recently, we have shown that multifrequency EPR and particularly EPR at high magnetic fields (ca. >3 T) offers a new and sensitive route to measure zero field splitting of Gd(III) chelates in water and to probe water interactions and chelates dynamics.<sup>1,2</sup> The method we developed (*ibid.*) is based on the Hudson and Lewis approach.<sup>3</sup> A similar treatment was developed by Merbach and co-workers.<sup>4</sup> In order to obtain a satisfactory fit of EPR data, both the Urbana and the Switzerland groups included a frequency-independent

relaxation term which is thought to arise from spin rotation. The only way to confirm this mechanism is to study Gd(III) EPR above the resonance frequencies of 250 GHz.

Using unique high field EPR instrumentation developed at the NHMFL we have obtained room-temperature EPR spectra from aqueous 5 mM solutions of two common MRI contrast agents—Gd-DOTA and a pentane derivative of this chelate—Gd-DOTAP. Combined line width data for these chelates are shown in Figure 1 (after correction for concentration dependence). It is clear that up to 330 GHz experimentally observed line widths remain above the predicted frequency independent value (shown as dashed line). Although current observations agree with our theory, measurements at higher resonance frequencies (at least 400 to 500 GHz) are needed to understand this relaxation effect. We suspect that the frequency-independent line width of ca. 5 G for these complexes is unusually large and that, perhaps, some of this width is due to rotational modulation of not fully isotropic Zeeman terms. If this is the case, the width will increase at higher magnetic field, providing a new route to study these medically-important S-state ion chelates.

Another set of experiments carried out with frozen solutions of Gd-chelates was aimed at determining the number of molecules in the first coordination sphere of these complexes by analyzing spectral broadening in the presence of O<sup>17</sup> enriched water. This information is impossible to obtain at conventional EPR frequencies and even at 95 GHz because the lines are broad and complex. Even ENDOR and ESEEM X-band data is difficult to analyze unambiguously because of the large zero field splitting effects. At magnetic fields corresponding to 330 to 440 GHz and higher, the rigid limit spectra from Gd chelates are significantly simplified and are between 12 and 40 G wide. Figure 2 shows a sample of changes in 330 GHz EPR spectra from Gd-EDTA upon substituting water to 37% O<sup>17</sup> enriched H<sub>2</sub>O. The spectra were double-integral-normalized to demonstrate effects of broadening by hyperfine interaction with O<sup>17</sup> isotope. We used a spectral subtraction method of Reed and coworkers<sup>5</sup> to estimate

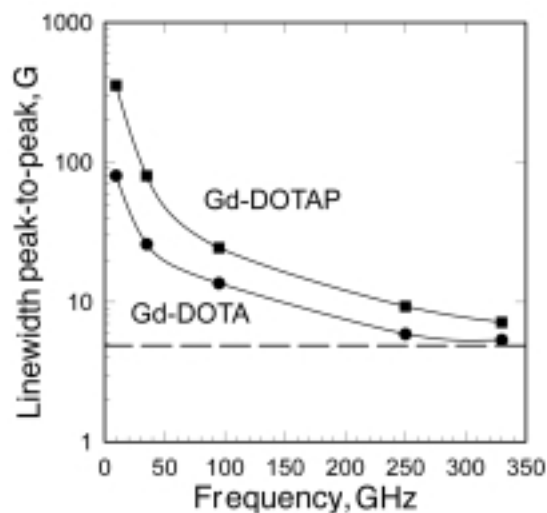


**Figure 1.** Linewidth of the EPR spectra versus frequency for two common MRI contrast agents.

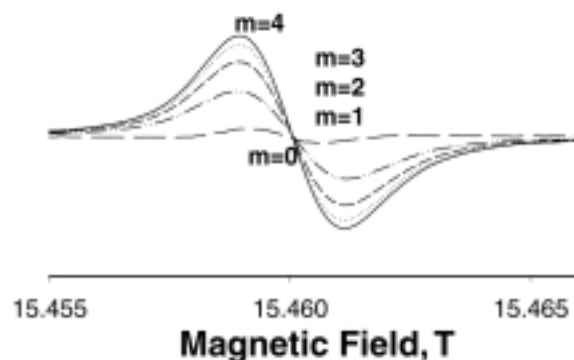


**Figure 2.** EPR lineshape of Gd-EDTA for different number of H<sub>2</sub>O molecules in the first coordination shell (see text).

the number of water molecules in the first coordination sphere of the ion and the magnitude of the hyperfine splitting constant (the application of spectral subtraction method is demonstrated at the bottom of Figure 2). The O<sup>17</sup> coupling constant we estimate from these measurements (0.3 G) agrees well with indirect data reported in Ref. 4. Thus, further ENDOR studies of these chelates carried out at high magnetic fields will give detailed geometrical information about water coordination in these complexes.

- 1 Smirnova, T.I., *et al.*, J. Am. Chem. Soc., **120**, 5060 (1998).
- 2 Clarkson, R.B., *et al.*, Molec. Phys., **95**, 1325 (1998).
- 3 Hudson, A., and Lewis, J.W., Trans. Faraday Soc., **66**, 1297 (1969).
- 4 Powell, P.D., *et al.*, J. Am. Chem. Soc., **118**, 9333 (1996).
- 5 Kofron, J.L., *et al.*, Biochem., **27**, 4781 (1992); Latwesen, D.G., *et al.*, Biochem., **31**, 9608 (1992).

## Initial Structural Characterization of the Intact M2 H<sup>+</sup> Channel Protein

Tian, C., FSU, Molecular Biophysics

Tobler, K., Northwestern Univ., Biochemistry, Molecular Biology & Cell Biology

Lamb, R., Northwestern Univ., Biochemistry, Molecular Biology & Cell Biology

Cross, T.A., NHMFL/FSU, Chemistry and Molecular Biophysics

The transmembrane ion channel formed by a tetramer of the M2 protein from influenza A virus plays an important role in viral infection. To reveal the structure and understand the functional properties of this membrane protein we have uniformly <sup>15</sup>N labeled intact M2 protein for solid state NMR experiments. The protein has been expressed in *E. coli* using a construction with a T7 promoter and induction by IPTG. The expressed protein has been purified by affinity chromatography and purity has been checked by electrophoresis. With detergent (SDS) solubilization the intact M2 protein can be induced to incorporate into preformed liposomes. After spreading proteoliposome aliquots

on glass slides and air drying, a well-oriented sample for solid-state NMR can be obtained following overnight incubation at 93% humidity and 43 °C.

Preliminary PISEMA solid-state NMR spectra of uniformly  $^{15}\text{N}$  labeled M2 protein is shown in the figure. Even from this early spectrum it is clear that sharp resonances are achievable, meaning that very well oriented protein is present in the sample. As yet it is not certain that all of the resonances are identifiable, however, much of the intensity appears in the region around 60 ppm in the chemical shift dimension and  $\pm 5$  kHz in the  $^{15}\text{N}$ - $^1\text{H}$  dipolar dimension. This region is primarily associated with alpha-helical portions of the protein on the membrane surface. In contrast, intensity in the broad region around 150 ppm and  $\pm 10$  kHz is associated with helices that span the bilayer and hence have a relatively small angle between the bilayer normal and the helix axis.

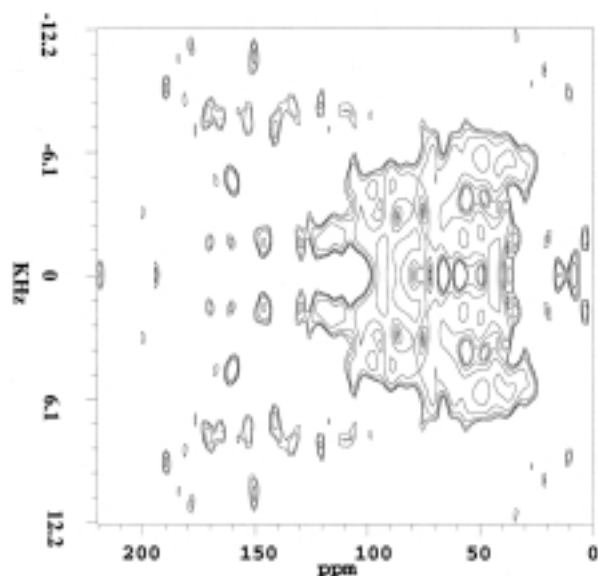


**Figure 1.**  $^{15}\text{N}$  PISEMA spectrum obtained from a uniformly hydrated sample of M2 protein in well oriented dimyristoylphosphatidyl-choline bilayers.

## Uniform Alignment of the *Streptomyces* $\text{K}^+$ Channel

Tian, C., FSU, Molecular Biophysics

Mo, Y., FSU, Chemistry

Wang, J., FSU, Molecular Biophysics

Miller, C., Brandeis Univ., Biochemistry

Cross, T.A., NHMFL/FSU, Chemistry and Molecular Biophysics

KcsA protein from *Streptomyces* is the simplest known potassium channel. This protein is much smaller than any known eukaryotic pore forming subunits, containing only 160 amino acid residues. The structure of KcsA has been determined by X-ray crystallography at a resolution of 3.2Å revealing that this channel is a tetramer with a four-fold axis of molecular symmetry around the central ion conducting pore.

The monomeric unit consists of two transmembrane helices and a short helix directed toward the aqueous cavity at the bilayer center. The selectivity filter is lined with backbone carbonyl oxygens in much the same way that the gramicidin channel is lined. Before a detailed understanding of ion selectivity and conductance efficiency can be achieved, however, high resolution structure and dynamic information is needed. To obtain this information from solid state NMR we have prepared uniformly aligned samples of the KcsA protein in lipid bilayers.

The protein has been solubilized in *E. coli* lipid extracts using the detergent (CHAPS) mediated reconstitution method. After successful reconstitution the proteolipid sample is diluted to an appropriate concentration and dispersed by mild sonication, then freeze thaw cycles are used to obtain high quality proteoliposomes. After several rounds of sonication-freeze-thaw, the sample is dispensed to glass slides, air-dried, and then hydrated in a 93% relative humidity chamber at 43 °C overnight. The hydrated samples on glass slides are then placed in a square glass tube and sealed. Orientation of the lipid bilayers was checked by  $^{31}\text{P}$  NMR as shown in the figure.

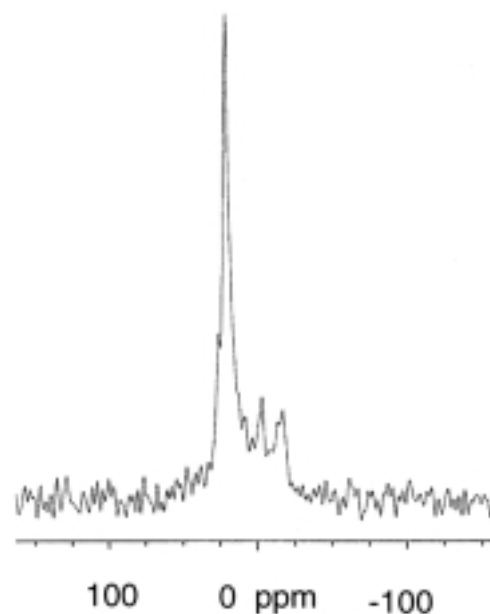


**Figure 1.**  $^{31}\text{P}$  NMR spectra obtained in a 300 MHz NMR spectrometer showing small isotropic and powder pattern sample portions and a dominate signal intensity from the portion of the sample aligned with the bilayer normal parallel to the magnetic field direction.

## Structural Studies of Monomeric Forms of the Diphtheria Toxin Repressor in Solution

Twigg, P.D., FSU, Biophysics

Wylie, G.P., FSU, Chemistry

Caspar, D.L.D., FSU, Biology and Biophysics

Murphy, J.R., Boston Univ., Medicine

Logan, T.M., NHMFL/FSU, Chemistry

The diphtheria toxin repressor (DtxR) is a 226 amino acid protein that regulates expression of diphtheria toxin and other iron-regulated proteins in the Gram-positive bacterium *Corynebacterium diphtheriae*. A working model for regulation by iron has been proposed in which the repressor exists as a monomer, incapable of DNA binding in the absence of iron. Upon introduction of the physiological ligand,  $\text{Fe}^{2+}$ , DtxR dimerizes, binds metal, and binds DNA in a sequence-specific manner, shutting off synthesis of the diphtheria toxin. This model is based on genetic and physiological data, but structural studies are not in complete agreement with this model. In this project, we are using multidimensional heteronuclear magnetic resonance to investigate the solution structure of monomeric DtxR in an effort to better understand the transition between “active” and “inactive” forms of the repressor protein.

A key to our research was the serendipitous discovery that a modified version of DtxR that contains three additional residues at the N-terminus (gshDtxR) binds iron like wild-type DtxR, but does not dimerize or bind DNA. Interestingly, this protein crystallizes into the same space group as the wild-type DtxR in the absence of metal, indicating that many of the previous structural studies, performed using crystallography, may be affected by crystal packing constraints. Studies to date indicate that the solution structure of gshDtxR differs considerably from that observed in the crystal. Figure 1 shows a 2D  $^1\text{H}$ ,  $^{15}\text{N}$  correlation spectrum (HSQC) collected on gshDtxR that is uniformly labeled in  $^{15}\text{N}$ . This 2D spectrum gives correlations between the amide proton and nitrogen for each residue in the protein. For our construct, we expect ~220 resonances (prolines don't contain NH bonds), but we clearly see significantly fewer than this number. Specifically, the resonances that are observed can be assigned by inspection to the C-terminal ~80 amino acid residues of gshDtxR. Other studies have demonstrated that this spectrum does not change upon refolding or treatment with EDTA. Upon complete denaturation, we obtain a spectrum consistent with an unfolded protein of approximately 226 amino acid residues. From these data we tentatively conclude that the N-terminal domain of gshDtxR exists in a conformationally averaged state, possibly similar to a molten globule, that adopts an ordered conformation upon dimerization. CD spectra indicate extensive secondary structure formation in monomeric gshDtxR, and we are currently pursuing additional studies to further define the nature of this protein in solution.

Acknowledgements: This work was supported by NIH, the American Heart Association, and NSF.

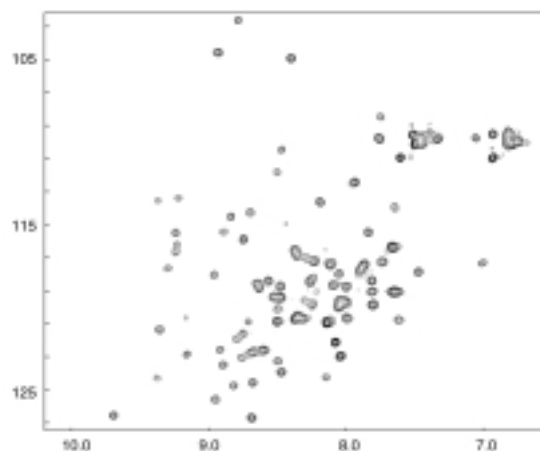


Figure 1. 2D HSQC spectrum of gshDtxR (229 amino acid residues).

## Manipulation of Cell Division Using Static Magnetic Fields

Valles, Jr., J.M., Brown Univ., Physics

Wasserman, S., Brown Univ., Physics

Liu, J., Brown Univ., Physics

Denegre, J.M., Brown Univ., Molecular Biology, Cell Biology, and Biochemistry

Mowry, K.L., Brown Univ., Molecular Biology, Cell Biology, and Biochemistry

We performed a series of experiments to investigate the mechanisms responsible for the magnetic field induced alteration of the early cell divisions in eggs of the frog, *Xenopus laevis*. The work consisted of timing experiments, *in situ* visualization measurements, and *ex situ* visualization measurements. In the timing experiments we varied the time interval during which the frog eggs were exposed to the field in order to determine the window of maximum sensitivity. While we succeeded in determining how long and when to put the eggs in to achieve the largest number of altered cell divisions, the result surprised us. The third cell divisions are the ones altered by field, but the most sensitive time ends long before this division. We developed a microscope/camera system that worked in the large bore magnet to watch the eggs while they developed in the magnetic field. The goal was to detect any overall changes in the shape of the eggs and to observe the cell divisions while they happened. We were successful on both fronts. Notably, we found that a large magnetic field does not alter the shapes of the large (1 mm diameter) eggs. Finally, we fixed eggs that had been exposed to magnetic field so that we could perform microscopy on them to determine which internal structures involved in cell division are altered by a magnetic field. This portion of the work is ongoing.

We are in the process of writing up our timing results and a description of the microscope apparatus.



## NMR Studies of Backbone Motions of Proteins That Affect Cancer Progression

Van Doren, S.R., Univ. of Missouri-Columbia,  
Biochemistry

Gao, G., Univ. of Missouri-Columbia, Biochemistry

Human tissue inhibitors of metalloproteinases (TIMPs) slow tumor growth and slow the development of the blood vessels required to support tumors. These effects are likely mediated by their inhibition of matrix metalloproteinases, which are agents of tissue remodeling by way of hydrolysis of proteins of the extracellular matrix. The relaxation of NMR-detected  $^{15}\text{N}$  magnetization is employed to identify amplitudes and timescales of internal motions of the backbone of proteins. The timescales accessible in solution are typically picoseconds to nanoseconds and microseconds to milliseconds. Spin-spin ( $T_2$ ) relaxation is sensitive to the latter, slower motions. The spin-spin relaxation of the microsecond to millisecond-scale motions can be dramatically enhanced by increasing the magnetic field.  $^{15}\text{N}$   $T_1$ ,  $T_2$  and  $^{15}\text{N}\{^1\text{H}\}$ NOE measurements of human N-TIMP-1 were collected on the NBMFL 720 MHz NMR spectrometer in November 1999. Preliminary interpretation of the 720 MHz data appears to confirm Missouri's 500 MHz evidence for microsecond to millisecond motions. The sites of these motions (light colored areas in the backbone bundle pictured in Figure 1) lie at or near the sites of MMP-dependent conformational change in the MMP-binding ridge of N-TIMP-1 seen in the NMR structure of Wu *et al.*<sup>1</sup>

The tumor antigens of DNA tumor viruses such as SV40 and polyomavirus possess an N-terminal DnaJ-like co-chaperone domain that facilitates cellular transformation, cell cycle progression, DNA replication, and propagation of the virus. We

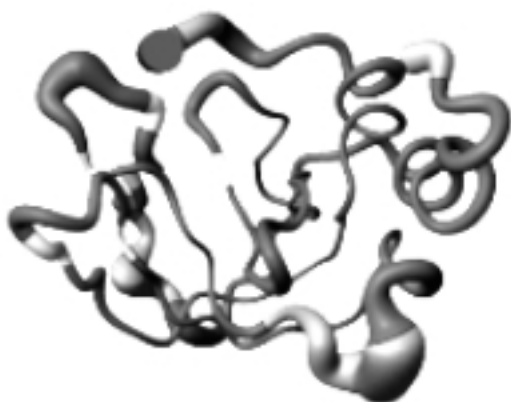


**Figure 1.** Human TIMP-1 structure with sites of slow motions, important for function, more obvious at high magnetic field marked with the light color.

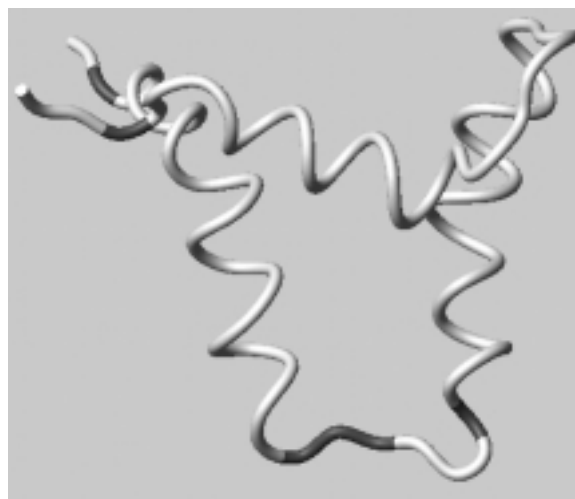


**Figure 2.** Portion of a tumor virus antigen with sites of functional, fast motions at bottom of figure.

have found the loop to be rich in picosecond to nanosecond motions (dark section in the low resolution model, Figure 2), as evident from  $^{15}\text{N}$   $T_1/T_2$  ratio and  $^{15}\text{N}\{^1\text{H}\}$ NOE measurements. The fast motions are presumably important in the tumor viral co-chaperone's interaction with the hsc70 co-chaperone and stimulation of its ATPase activity, since the unrestricted fast motions prevail in the universally conserved HPD loop at bottom in the picture of the structure.

<sup>1</sup> Wu, B., *et al.*, "NMR Structure of Tissue Inhibitor of Metalloproteinases-1 Implicates Localized Induced Fit in Recognition of Matrix Metalloproteinases," *J. Mol. Biol.*, **295**, 257-268 (2000).

## Structure and Possible Function of the C-Terminal Domain of the Diphtheria Toxin Repressor

Wang, G.-S., FSU, Biophysics

Wylie, G.P., FSU, Chemistry

Twigg, P.D., FSU, Biophysics

Caspar, D.L.D., FSU, Biology and Biophysics

Murphy, J.R., Boston Univ., Medicine

Logan, T.M., NBMFL/FSU, Chemistry

The diphtheria toxin repressor (DtxR) is the best characterized member of a family of homologous proteins that regulate iron uptake and virulence gene expression in the Gram positive bacteria. DtxR contains two domains that are separated by a short, flexible linker of approximately 10 amino acid residues. The N-terminal domain (130 aa residues) is structurally well-

defined and is responsible for Fe<sup>2+</sup>-binding, dimerization, and DNA binding. A partial X-ray crystallographic structure demonstrated that the C-terminal domain (80 aa residues) is structurally similar to eucaryotic SH3 domains, but the functional role of this domain in repressor activity was unknown. In this project, we used multidimensional heteronuclear NMR methods to obtain complete, sequential chemical shift assignments, and to determine a high-resolution structure of residues 130-226 of the intact repressor in solution (Figure 1). Residues preceding A147 were highly mobile in solution and adopted a random coil conformation. Residues A147-L226 form an independently-folding domain consisting of five  $\beta$ -strands and three helices arranged into a partially orthogonal, two-sheet  $\beta$ -barrel, similar to the structure observed in the crystalline Co<sup>2+</sup>-bound complex of full-length DtxR, and to that of eucaryotic SH3 domains.

SH3 domains are small proteins that mediate protein-protein interactions that occur to regulate protein activity and signal transduction in eucaryotic cells by binding to proline-rich regions of proteins. Proteins structurally homologous to SH3 domains had previously been identified from prokaryotic sources, but their functional roles were not identified. We used chemical shift perturbation studies to demonstrate that a proline-rich peptide corresponding to residues R125- G139 of intact DtxR binds to the C-terminal domain in a pocket formed by residues in  $\beta$ -strands 2, 3, and 5, and in helix 3. Binding of the proline-rich peptide by the C-terminal domain of DtxR represents the first demonstration of a functional

SH3-like domain in a prokaryotic organism, and suggests that the C-terminal domain functions to regulate repressor activity. The strong sequence homology between DtxR and other members of this protein family, which includes virulence proteins from organisms causing tuberculosis, syphilis, and leprosi, suggests that our model, if valid, represents a general regulatory phenomenon. This model for regulation by the C-terminal domain of DtxR also suggests novel routes to the development of nonmetal-ion activators of repressor activity, which should decrease the virulence of these organisms.

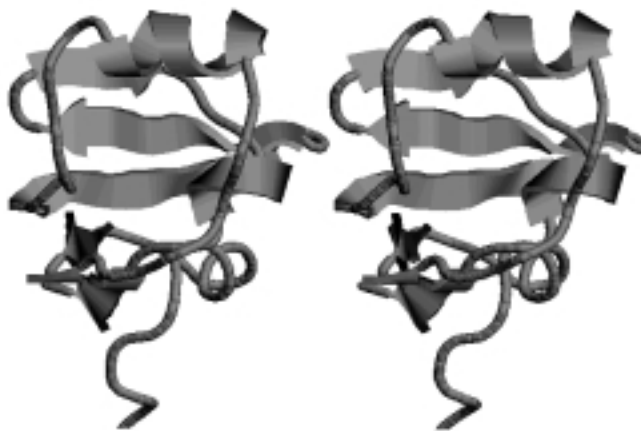


**Figure 1.** Structure of residues 130-226 of DtxR. A stereodialog is shown. To view the structure in stereo, slightly cross your eyes until the images line up and appear in 3D.

## CHEMISTRY

### Characterization of a Single Crystal Cubic Prussian Blue $\text{Co}_8(\text{tacn})_8(\text{CN})_{12}$ Cluster by Ion Trap and Fourier Transform Ion Cyclotron Resonance Mass Spectrometry with Microelectrospray Ionization

Andersen, U.N., Univ. of California at Berkeley, Chemistry  
König, S., UC Berkeley, Chemistry  
Leary, J.A., UC Berkeley, Chemistry  
Freitas, M.A., NHMFL  
Marshall, A.G., NHMFL/FSU, Chemistry

A single crystal of  $\text{Co}_8(\text{tacn})_8(\text{CN})_{12}$  has been characterized by micro-electrospray mass spectrometry. Because a crystal is inherently purer than the solution in which the crystals form, the mass spectrum is inherently simpler and more readily resolved

and interpreted. The spectra obtained by use of FT-ICR, ion trap and quadrupole mass spectrometers show the +4, +3 and +2 charge states of the cluster. With the aid of a 9.4 T FT-ICR mass spectrometer it was possible to resolve the isotope pattern for each individual charge state. The data collected suggest that micro-electrospray renders spectra that are more specific to the intact molecule, whereas more fragmentation is induced under normal electrospray conditions. The present data suggest that micro-electrospray is a powerful tool for characterization of compounds that can be crystallized.

**Acknowledgements:** The authors acknowledge Prof. Jeffrey R. Long, Polly A. Berseth, and Julie L. Heinrich for synthesis of the compound presented herein. A. G. Marshall and M. A. Freitas also thank the NSF National High Field FT-ICR Mass Spectrometry Facility (CHE-94-13008), Florida State University, and the NHMFL at Tallahassee, Florida for their financial support.

<sup>1</sup> Andersen, U.N., *et al.*, J. Am. Soc. Mass Spectrom., **10**, 352-354 (1999).